AGU PUBLICATIONS

JGR

Journal of Geophysical Research: Solid Earth

RESEARCH ARTICLE
10.1002/2014JB011561

Key Points:
- Thin continental crust underlies most of the Santos Basin/São Paulo Plateau
- Atypical velocity structure of its central domain unveils early rifting episode
- Segmentation shows rifting was oblique to opening direction of South Atlantic

Supporting Information:
- Figures S1–S8 and Tables S1–S5

Correspondence to:
M. Evain,
mikael.evain@ifremer.fr

Citation:
Evain, M., et al. (2015), Deep structure of the Santos Basin-São Paulo Plateau System, SE Brazil, *J. Geophys. Res. Solid Earth*, *120*, doi:10.1002/2014JB011561.

Received 28 AUG 2014
Accepted 8 JUL 2015
Accepted article online 14 JUL 2015

Deep structure of the Santos Basin-São Paulo Plateau System, SE Brazil

M. Evain[1], A. Afilhado[1,2,3], C. Rigoti[4], A. Loureiro[2], D. Alves[2], F. Klingelhoefer[1], P. Schnurle[1], A. Feld[1], R. Fuck[5], J. Soares[5], M. Vinicius de Lima[6], C. Corela[2], L. Matias[2], M. Benabdellouahed[1,7], A. Baltzer[1,8], M. Rabineau[7], A. Viana[4], M. Moulin[1], and D. Aslanian[1]

[1]Ifremer, Géosciences Marines, Technopôle Brest-Iroise, Plouzané, France, [2]Instituto Dom Luis, Faculdade de Ciências da Universidade de Lisboa, Lisbon, Portugal, [3]Instituto Superior de Engenharia de Lisboa, Rue Conselheiro Emidio Navarro, Lisbon, Portugal, [4]PETROBRAS/CENPES-PROFEX, Rio de Janeiro, Brazil, [5]Lablithos, Instituto de Geociências, Universidade de Brasilia, Campus Darcy Ribeiro, Brasilia, Brazil, [6]Universidade Federal do Pampa, Campus Caçapava do Sul, Caçapava do Sul, Brazil, [7]Institut Universitaire Européen de la Mer, Domaines Océaniques, CNRS, Plouzané, France, [8]LETG-Nantes Géolittomer, Université de Nantes, Campus Tertre, Nantes, France

Abstract The structure and nature of the crust underlying the Santos Basin-São Paulo Plateau System (SSPS), in the SE Brazilian margin, are discussed based on five wide-angle seismic profiles acquired during the Santos Basin (SanBa) experiment in 2011. Velocity models allow us to precisely divide the SSPS in six domains from unthinned continental crust (Domain CC) to normal oceanic crust (Domain OC). A seventh domain (Domain D), a triangular shape region in the SE of the SSPS, is discussed by Klingelhoefer et al. (2014). Beneath the continental shelf, a ~100 km wide necking zone (Domain N) is imaged where the continental crust thins abruptly from ~40 km to less than 15 km. Toward the ocean, most of the SSPS (Domains A and C) shows velocity ranges, velocity gradients, and a Moho interface characteristic of the thinned continental crust. The central domain (Domain B) has, however, a very heterogeneous structure. While its southwestern part still exhibits extremely thinned (7 km) continental crust, its northeastern part depicts a 2–4 km thick upper layer (6.0–6.5 km/s) overlying an anomalous velocity layer (7.0–7.8 km/s) and no evidence of a Moho interface. This structure is interpreted as atypical oceanic crust, exhumed lower crust, or upper continental crust intruded by mafic material, overlying either altered mantle in the first two cases or intruded lower continental crust in the last case. The deep structure and v-shaped segmentation of the SSPS confirm that an initial episode of rifting occurred there obliquely to the general opening direction of the South Atlantic Central Segment.

1. Introduction

The Santos Basin-São Paulo Plateau System (SSPS) stands along the southeast Brazilian margin (Figure 1). It is situated immediately north of the Florianópolis (or Rio Grande) Fracture Zone (FFZ), which corresponds to one of the fundamental structures in the South Atlantic development. It separates two main geodynamic domains in the South American continental margins [*Moulin et al*., 2010, 2012; *Heine et al*., 2013]: a magma-rich domain to the south (Austral Segment), characterized by large and continuous seaward-dipping reflectors (SDRs), and an evaporitic sedimentary domain to the north (Central Segment), which is a moderately magmatic continental margin (inset in Figure 1). The SSPS has been interpreted as a kinematic "buffer" by *Moulin et al*. [2012]: while the southern Austral Segment opened between the anomalies M13 and M4 [*Rabinowitz and Labrecque*, 1979; *Austin and Uchupi*, 1982; *Curie*, 1984; *Moulin et al*., 2010; *Heine et al*., 2013], respectively 139.5 Ma and 130 Ma [*Gradstein et al*., 2004], the oceanic spreading in the Central Segment started more than 18 Ma later, at the end of evaporite deposition (Upper Aptian-Lower Albian: 112 Ma) [*Rabinowitz and Labrecque*, 1979; *Curie*, 1984; *Torsvik et al*., 2009; *Moulin et al*., 2010]. This buffer situation, inducing the referred time delay, may coincide with the location of a "second-order intraplate boundary" as defined by *Olivet et al*. [1984] in relationship with the Paraná-Etendeka Continental Flood Basalts [*Curie*, 1984; *Unternehr et al*., 1988; *Nürnberg and Müller*, 1991]. The particular situation gives a rhombus shape to the SSPS, bounded by the FFZ, the Cruzeiro do Sul and the Capricórnio lineaments, and the Brazilian coast.

A first exploration phase of the SSPS was made in the 1970s. Several multidisciplinary studies were conducted in the area, including seismic reflection and refraction surveys, gravity and magnetic measurements, seafloor sampling, and integration with onshore and shallow offshore well information available at that time. This first

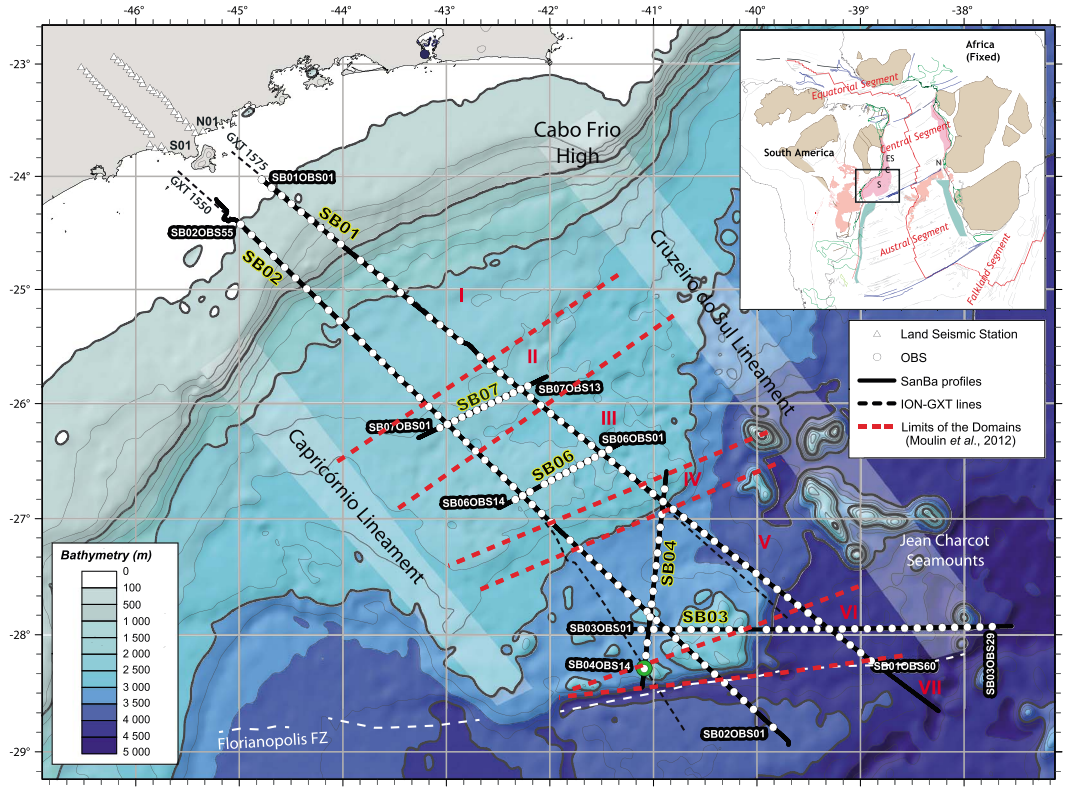

Figure 1. Predicted bathymetry [*Smith and Sandwell*, 1997] of the Santos Basin-São Paulo Plateau System (SSPS) and location of the seismic profiles of the SanBa (SB) experiment, SB01 to SB07. Seismic profiles are indicated by thick black lines, OBS in white circles, and land seismic station in white triangles. Dashed red lines are the limits of Domains I to VII proposed by *Moulin et al.* [2012]. A green circle shows DSDP site 356 (also the location of OBS SB04OBS14). Inset: Adapted tectonostructural map of the South Atlantic Ocean at Chron 34 (84 Ma) from *Moulin et al.* [2012] showing the main segmentation in the South Atlantic. Study area within the black square; brown: cratons; pink: Aptian salt; red: Cretaceous volcanism; green: SDR (seaward-dipping reflectors); S: Santos Basin; C: Campos Basin; ES: Espírito Santo Basin; N: Namibian basin.

exploration phase was concluded by a Deep Sea Drilling Project (DSDP) drilling (Leg 39, Site 356) [*Perch-Nielsen et al.*, 1977] on the São Paulo Ridge (SE of the SSPS, Figure 1). Key results related to these investigations were recently summarized by *Kumar et al.* [2012]:

1. The sedimentary wedge in the Santos basin deep water (beyond the 200 m isobath) as well as further north in the Espírito Santo and Campos basins is at least 4–6 km thick and locally thins over basement highs [*Kumar et al.*, 1977].
2. The extensive field of diapiric structures was deemed to be salt diapirs [*Leyden et al.*, 1976, 1978].
3. A refraction experiment made from sonobuoy measurements indicates that the Moho at the center of the São Paulo Plateau is at a depth of about 15 km [*Leyden et al.*, 1971]. Despite a large crustal thickness (~10 km; note here that by crust and crustal thickness, we consider in this study solely the crystalline part of the crust, without its sedimentary cover), *Leyden et al.* [1971] suggested that the nature of the crust was oceanic. To date, these are the only seismic refraction data published in this area.
4. Based on seismic data and drilling results from the DSDP hole 356 in the São Paulo Ridge [*Perch-Nielsen et al.*, 1977], *Kumar et al.* [1977], and *Kumar and Gambôa* [1979] correlated the postsalt stratigraphy across the SSPS to the edge of the continental shelf. In order to account for a ~600 km wide plateau, they invoked an eastward ridge jump at the end of Aptian time.

A second phase was conducted in 2006 after the discoveries of presalt giant oil reserves in the Santos Basin. Modern seismic data acquired and processed by ION-GXT imaged the Moho from thick continental crust (>30 km) to thin oceanic crust (~5 km). Based on this data set, two recent studies came to different conclusions on the crustal architecture of the SSPS:

1. *Zalán et al*. [2011] interpret the continental crust beneath the whole SSPS. The authors claim that a strong continuous reflector, the Conrad discontinuity, separates the crust between a rigid, highly fractured upper part and a ductile lower part. The São Paulo Plateau is described as a 15 km thick continental crust topped by about 4 km of volcanic material. By analogy with the Iberian Margin, they interpret the easternmost part of the SSPS as exhumed mantle. This exhumed mantle is further supposed to surround the entire SSPS, including the São Paulo ridge, as well as the Campos and Espírito Santo basins.
2. *Kumar et al*. [2012], on the other hand, do not notice evidence of exhumed mantle, except, maybe, along the Florianópolis Fracture Zone, as it was described along other fracture zones such as the São Paulo (Romanche) Fracture Zone in the Equatorial Segment [*Seyler and Bonatti*, 1997; *Hekinian et al*., 2000]. Though *Kumar et al*. [2012] agree with *Zalán et al*. [2011] on the continental nature of the SSPS, they suggest, following *Thybo and Nielsen* [2009] and *Aslanian et al*. [2009], that extension might have been partly accomplished by volcanic intrusions and extrusions.

The recent kinematic study of *Moulin et al*. [2012] proposes that the São Paulo Plateau represents a microblock. Its own relative movement can account for the necessary divergence to form the wide SSPS and the narrow Namibe margin, which appears to be a transform margin. The divergent movement of the microblock also created the NW-SE trend of the two Capricórnio and Cruzeiro do Sul lineaments, interpreted as transfer zones [*Cobbold et al*., 2001; *Meisling et al*., 2001]. According to *Moulin et al*. [2012], whether a highly stretched continental crust is present beneath the SSPS or an episode of oceanic spreading occurred has similar implication in terms of horizontal movement. Following a different hypothesis for the genesis of passive margin, the formation of the SSPS can equally be explained by a phase of lower crust and/or upper mantle exhumation [*Péron-Pinvidic and Manatschal*, 2008; *Aslanian et al*., 2009; *Huismans and Beaumont*, 2011]. Therefore, by acquiring refraction/reflection seismic data, the 2011 Santos Basin (SanBa) experiment aimed at precisely imaging the deep structure of SSPS in order to specify the segmentation and unveil its nature.

2. The SanBa Experiment

The SanBa (Santos Basin) experiment was a joint project between the Laboratory of Geophysics and Geodynamics of Ifremer (Institut Français de Recherche pour l'Exploitation de la MER, France), the "Oceanic Domains" Laboratory of Institut Universitaire et Européen de la Mer, France, the University of Lisbon's Faculty of Sciences (IDL, Portugal), the University of Brasilia (Brazil), and Petrobras (Brazil). The project relied on the acquisition of bathymetric, chirp [*Baltzer et al*., 2014], and seismic data along key profiles in the SSPS.

The region of the SSPS where the experiment took place is bounded to the NE by the Cruzeiro do Sul Lineament that connects the Cabo Frio High and the Jean Charcot seamounts [*Gonçalves De Souza*, 1991; *Gonçalves De Souza et al*., 1993; *Mohriak and Szatmari*, 2008; *Mohriak et al*., 2010], to the SW by the Capricórnio Lineament [*Bueno et al*., 2004], and to the south by the São Paulo Ridge close to the Florianópolis Fracture Zone (Figure 1).

A segmentation of the SSPS in seven domains (Figure 1) was proposed by *Moulin et al*. [2012] who interpret them as follows:

1. Domains I and V consist of (thinned) continental crust.
2. Domains II and IV are either highly thinned continental crust or intruding/exhumed material.
3. Domain III is an abandoned oceanic ridge.
4. Domain VI remains uncertain. It forms a small triangle-shaped area at the SE end of the SSPS, in continuation of the São Paulo Ridge. Several previous studies proposed that most of the rocks in the southern part of the SSPS, near the Florianópolis Fracture Zone, correspond to basaltic layers [*Gladczenko et al*., 1997; *Mohriak*, 2004; *Mohriak and Szatmari*, 2008; *Blaich et al*., 2011], whereas some others proposed the presence of exhumed mantle [*Gomes et al*., 2009; *Zalán et al*., 2011]. Based on the recent analysis of one profile (SB03, Figure 1) from the SanBa seismic data set, *Klingelhoefer et al*. [2014] rule out a continental origin or exhumed serpentinized upper mantle material (clear reflections from the Moho) and propose that the crust underlying this domain is of oceanic origin.
5. Domain VII is oceanic crust.

The six multichannel (MCS) and coincident wide-angle seismic profiles aimed at imaging each of these seven domains (Figure 1). They were acquired between December 2010 and January 2011 by the R/V *L'Atalante*.

Profiles SB01 and SB02 strike in a NW-SE direction across all seven domains. They partly follow the tracks of two ION-GXT seismic lines separated laterally by less than a hundred kilometers. If a segmentation does exist, these two profiles should help in precisely characterizing the domain's boundaries and confirm the direction of opening of the SSPS. Each profile is more than 1000 km long. Between 55 and 60 ocean-bottom seismometers (OBS) and an additional 24 on-land seismic stations were deployed on each profile. The four remaining profiles all cross SB01 and SB02 and were dedicated to specific domains. The profile SB03 has a strictly east-west direction from the São Paulo Ridge (Domain V) to the oceanic crust (Domain VII). It aimed at unveiling the nature of Domain VI. This profile will not be detailed here as it has been the object of the specific article by *Klingelhoefer et al*. [2014]. SB04 is a 200 km long N-S profile perpendicular to SB03 designed to image both Domains IV and V and their expected structural transition. Fifteen OBS were deployed along this profile, the last one coinciding with the DSDP 356 site. At last, the SB06 and SB07 profiles are both 150 km long with 13 OBS. They run parallel to the segmentation to focus respectively on Domain III for SB06 and Domain II for SB07.

The Ifremer OBS pool (OldOBS and MicrOBS instruments) was used for offshore wide-angle seismic acquisition. Each OBS is equipped with a three-component geophone and a hydrophone. Onshore, portable seismic stations (Reftek 125A-01 and L-4C) from the Brazilian Geophysics Instrument pool (Observatório Nacional do Rio de Janeiro) were used. At each station position, three recording systems spaced 10 m apart were deployed in a triangle configuration. The seismic source consisted of a 8909 in 3 array of 18 air guns, towed 25 m below the sea level and fired every 60 s. Shots were also recorded by a 4.5 km long, 360-channel numerical streamer towed at 12–15 m depth 275 m behind the ship.

3. Data Processing and Modeling

Multichannel seismic (MCS) acquired jointly with refraction data was processed using the Geocluster (CGG Veritas) software. The processing sequence was composed of geometry, editing and water column mute, wide band-pass filtering (2–8–64–92 Hz), multichannel (shot gather) spiking predictive deconvolution (220 ms operator length, 66 ms lag), Common Mid Point sorting, velocity analysis, hyperbolic moveout multiple attenuation, spherical divergence compensation, time-variant band-pass filter (4–12–48–64 Hz at seafloor and 2–8–32–48 Hz from 4 s below seafloor), and prestack Kirchhoff time migration.

OBS data went through a three-stage preprocessing sequence including correction of internal clock drift to GPS base time, inversion of direct water wave arrivals to correct instrument position on the seafloor from a possible drift during its descent, and offset computation to edit and finalize SEGY files. Land station data went through a similar sequence without relocation. It was found that severe weather conditions affected the quality of numerous records, and valuable data were only recovered at land stations 1, 3–13, 18, and 21 along SB01 and land stations 1, 2, 5, 6, 8, and 9 along SB02.

Travel time picking was mostly performed on unfiltered refraction data to keep arrival times unchanged. A signal processing sequence was applied to help the picking of large-offset traces. It included debiasing, spectral deconvolution, a 5 to 15 Hz Butterworth filter and equalization (S. Operto, personal communication). Uncertainties were visually assigned according to the signal to noise ratio of traces. They were estimated to range between 50 and 100 ms.

Wide-angle data were modeled using the ray tracing and two-dimensional iterative damped least-squares travel time inversion of the RAYINVR software [*Zelt and Smith*, 1992; *Zelt*, 1999]. Modeling was performed using a layer-stripping approach, proceeding from the top of the structure toward the bottom. Arrival times of the main sedimentary and part of the crustal interfaces were picked on MCS lines from a joint interpretation of OBS and MCS main reflectors. They were converted to depth using velocities given by refracted phases of OBS data in order to build the velocity model. Geometric constraints provided by the MCS lines for postsalt, salt, presalt, and parts of the basement and Moho interfaces thus increased the reliability of the *P* velocity models. Interface depth and layer velocities were jointly adjusted until an acceptable fit with the OBS data was obtained and their consistency with MCS data verified. To avoid overparameterization of the inversion, only the reflectors identified in both the MCS and OBS data were included and lateral topographic or velocity changes inserted only where required by the data.

Besides this comparison between OBS data and MCS sections, several statistical parameters (i.e., number of picks, RMS, and χ^2, M. Loureiro et al., Monte Carlo approach to wide-angle model uncertainty assessment, submitted to *Tectonophysics*, 2015) and synthetic seismograms were also computed to validate modeling as it proceeded. A table of statistics for each line can be consulted in the supporting information (Tables S1–S5). Synthetic seismograms are shown below in parallel to recorded sections. They were created using the finite difference code of the Seismic Unix package [*Stockwell*, 1999]. A record length of 30 s at 100 m spacing and resampled velocity models at a lateral 50 m interval and a 10 m interval in depth were used. A Ricker wavelet source signal was parameterized centered at 8 Hz, similar to the signal from the air gun array used during the cruise.

In a postprocessing stage, further assessments were performed directly on final velocity models. A visual inspection of ray coverage and density plots is important to avoid overinterpretation of unconstrained regions in models (Figures S6a–S6e). An estimation of the resolution of every model is given in Figures S7a–S7e. More precisely, an a priori velocity error of 0.1 km/s and a depth error of 1 km were tested. As a first assessment of models' reliability, the lithospheric pressure was computed along models (Figures S8a–S8e). It was calculated at 125 km and did not exceed 50 MPa and therefore is still sustained by the crust [*Whitmarsh et al*., 1996].

4. Results

4.1. Profiles SB01 and SB02

SB01 and SB02 cross the entire SSPS. MCS data acquired along these profiles display a complex sedimentary structure and rough basement topography (Figures S1 and S2). One of the main feature is the salt that covers the whole northwestern part of the SSPS. It extends from the continental slope to OBS42 (530 km) on SB01 and to OBS24 (420 km) on SB02. There is a huge amount of sediments beneath the continental slope where the MCS shows several strong parallel reflectors, a few salt domes without a clear basement interface. In the oceanic basin, uppermost sediments either above the salt or covering the basement to the SE vary between 0.5 and 2 s twt (two way travel time). The salt is clearly underlain by a presalt layer of sediments between the continental slope and kilometer 260 on both profiles. Finally, an important difference in the sedimentary sequence of these two lines is the existence of a deep sedimentary basin along SB02 (between 450 and 550 km) that has no visible equivalent on SB01.

The top of basement reflection appears discontinuous on the MCS due to the effect of the salt and presalt topography. On both profiles, it is continuously rising toward the SE beneath presalt sediments. On SB01, it remains at about 5.5 s twt up to the crossing with SB07 and then goes down to ~6.5 s twt up to the end of the salt layer where it rises again and becomes a clearer and stronger reflector. On SB02, the basement goes slightly down to 5.5 s twt at the termination of the presalt and rises to ~5 s twt after 330 km. Its position is unclear beneath the deep sedimentary basin describe above, but from the crossing with SB04 toward the SE, the topography of the São Paulo Ridge and Fracture Zone is well imaged. Within the crust and deeper, the seismic signal is generally poor except after 700 km on SB01 where a horizontal reflector can be observed at about 10 s twt (see blue arrows in Figure S1).

4.1.1. Uppermost Sedimentary Structure

On OBS data (e.g., Figures 2–5), refracted phases in the uppermost sediments have apparent velocities varying between 2.0 and 3.5 km/s and are regularly seen among secondary arrivals at offsets between 5 and 15 km. On records from instruments located over the continental slope (OBS01 to OBS12 on SB01 and OBS55 to OBS45 on SB02), these phases evolve as first arrivals with velocities up to 4 km/s, indicating the thickening of these sediments toward the NW (e.g., Figure 4). Precritical reflections in the uppermost sedimentary sequence are usually seen beneath the direct water wave arrivals' cone of OBS data. They correlate well with the two uppermost sedimentary reflectors identified on the MCS lines (Figures S1 and S2).

These elements constrain the uppermost sedimentary structure of SB01 and SB02 velocity models (Figures 6 and 7). Both models are made of a first sedimentary layer, ~1 km thick, with velocities between 1.9 and 2.0 km/s. Below, the second layer is more heterogeneous as it depends on the salt and basement morphology. It is particularly thick (~3–4 km) with a high-velocity range (2.3–2.5 km/s at the top and 3.6–4 km/s at the bottom of the layer) over the continental slope area and between the large diapirs in the first kilometers of the oceanic basin (i.e., between 0 and 150 km). Seaward, it rarely exceeds 2 km above the salt for velocities varying from top

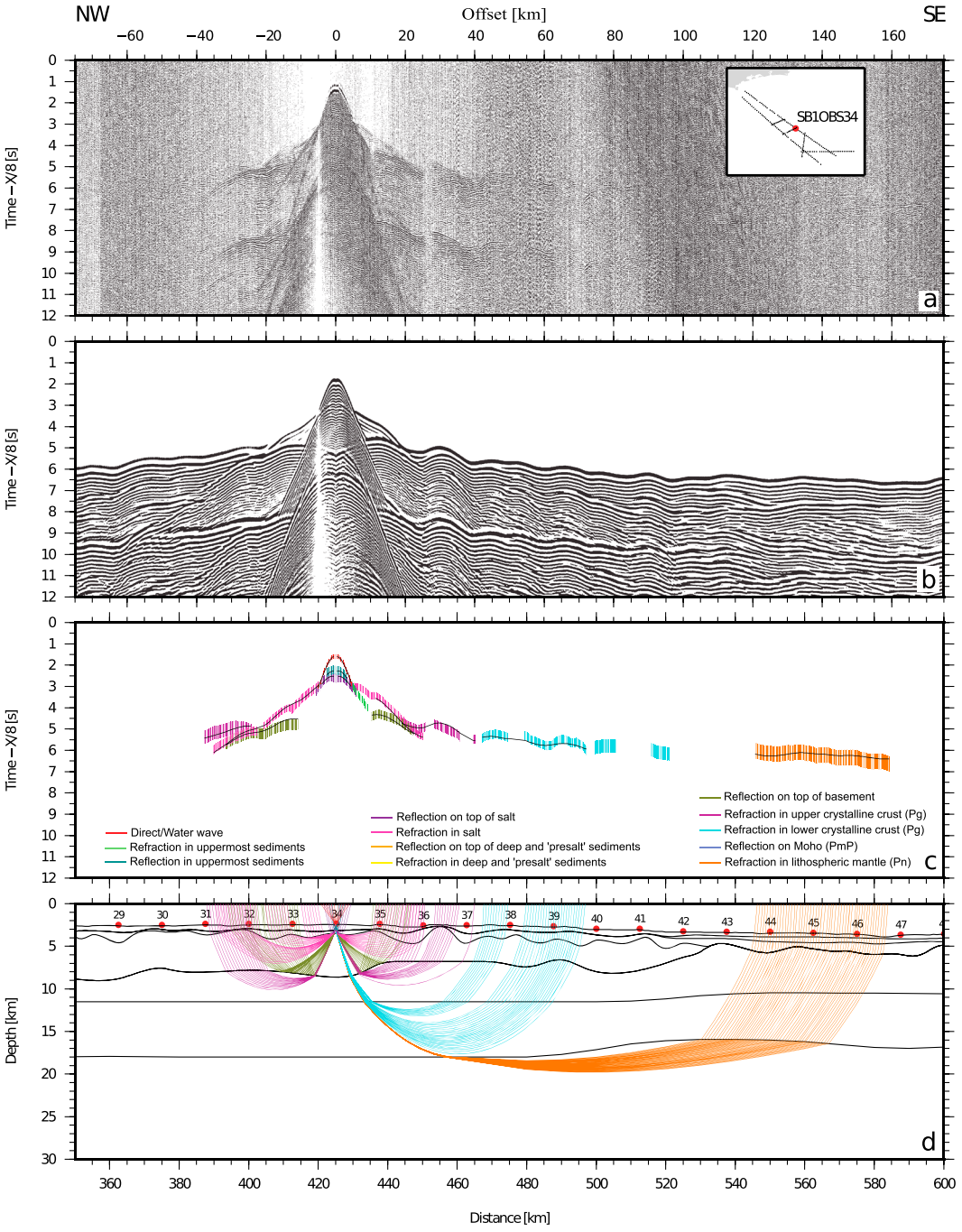

Figure 2. OBS34 on SB01 profile. (a) Geophone component of the recorded seismic section with band-pass filter (3–5–24–36), a 8 km/s velocity reduction, and an offset-dependent gain applied; (b) synthetic section [*Stockwell*, 1999] with the same velocity reduction and offset-dependent gain applied; (c) travel times picks from color-coded interpreted phases; black lines are calculated travel times in the final model; (d) corresponding ray tracing of black lines in Figure 2c.

to bottom between 2.3–2.5 km/s and 2.7–3.0 km/s. Along SB02, it thins to ~1 km above the deep sedimentary basin between 450 and 550 km, while its velocity range increases from 3.2 to 3.5 km/s as it drapes the rough basement at the termination of the line. On SB01, to the SE of the crossing with SB04, three sedimentary layers were modeled in good agreement with the MCS data (Figure S1). The second layer is very thin (less than 1 km) and has velocities of 2.2–2.4 km/s. Below, velocities in the third layer increase from 2.5–2.8 km/s at the top to 3.3–3.5 above the basement.

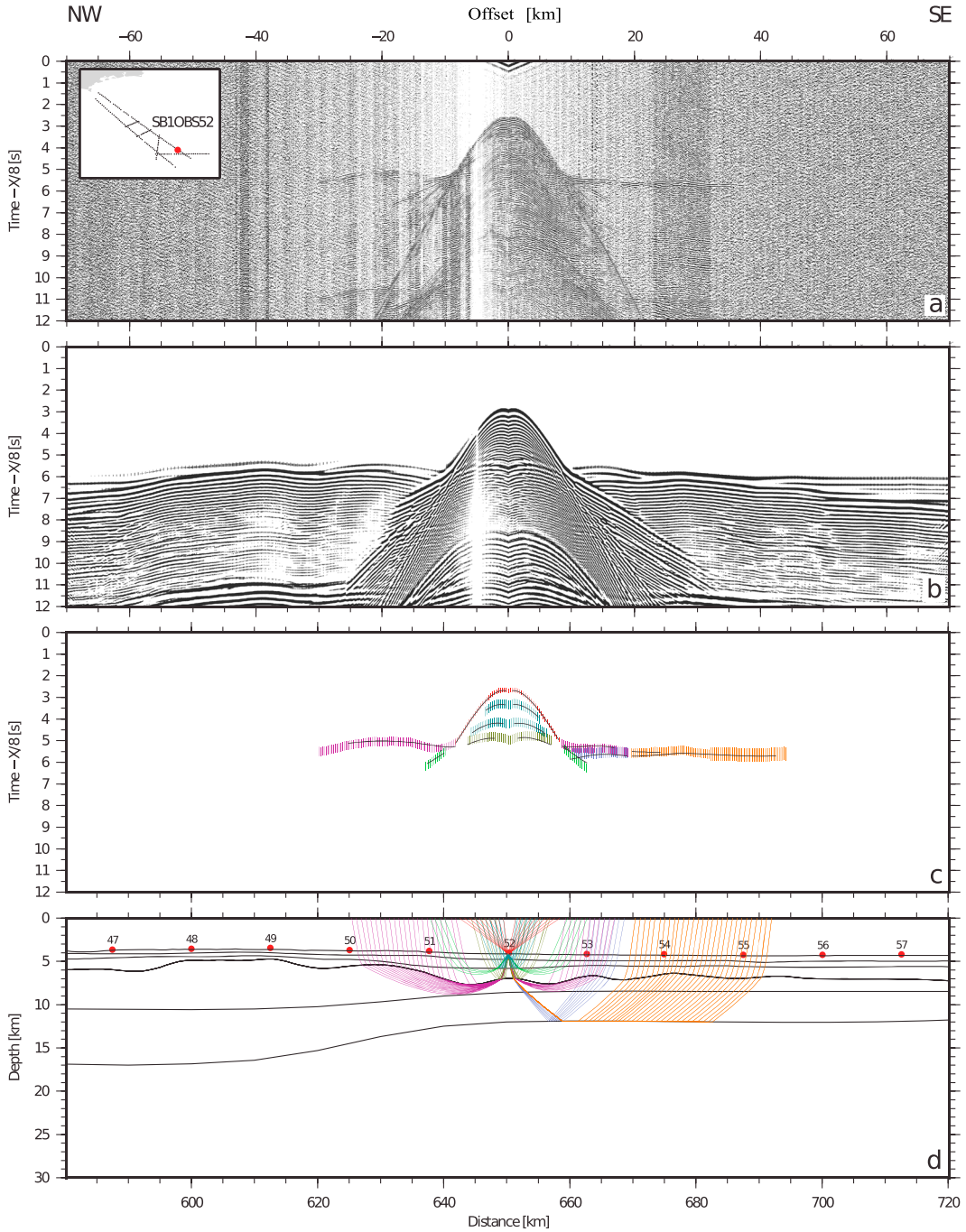

Figure 3. OBS52 on SB01 profile. Same legend and color code as Figure 2.

4.1.2. Deep Sedimentary Structure

The deep sedimentary structure of the SSPS consists of salt, presalt, and the deep basin observed on SB02. While, on SB02, a large salt diapir is present beneath the continental slope (km 60), on SB01, the first salt dome only appears at the termination of the slope (km 140). On this profile, instead of salt, MCS data suggest the presence of a thick accumulation of destabilized and deformed sediments (Figure S1). OBS data are, however, quite similar on both profiles with refracted phases that reach offsets as long as 40–50 km and apparent velocities increasing up to 5.5 km/s (Figure 4). The modeling of these phases implied a 10 km thick sedimentary package beneath the slope with velocities reaching 5.5–5.8 km/s at its deepest levels.

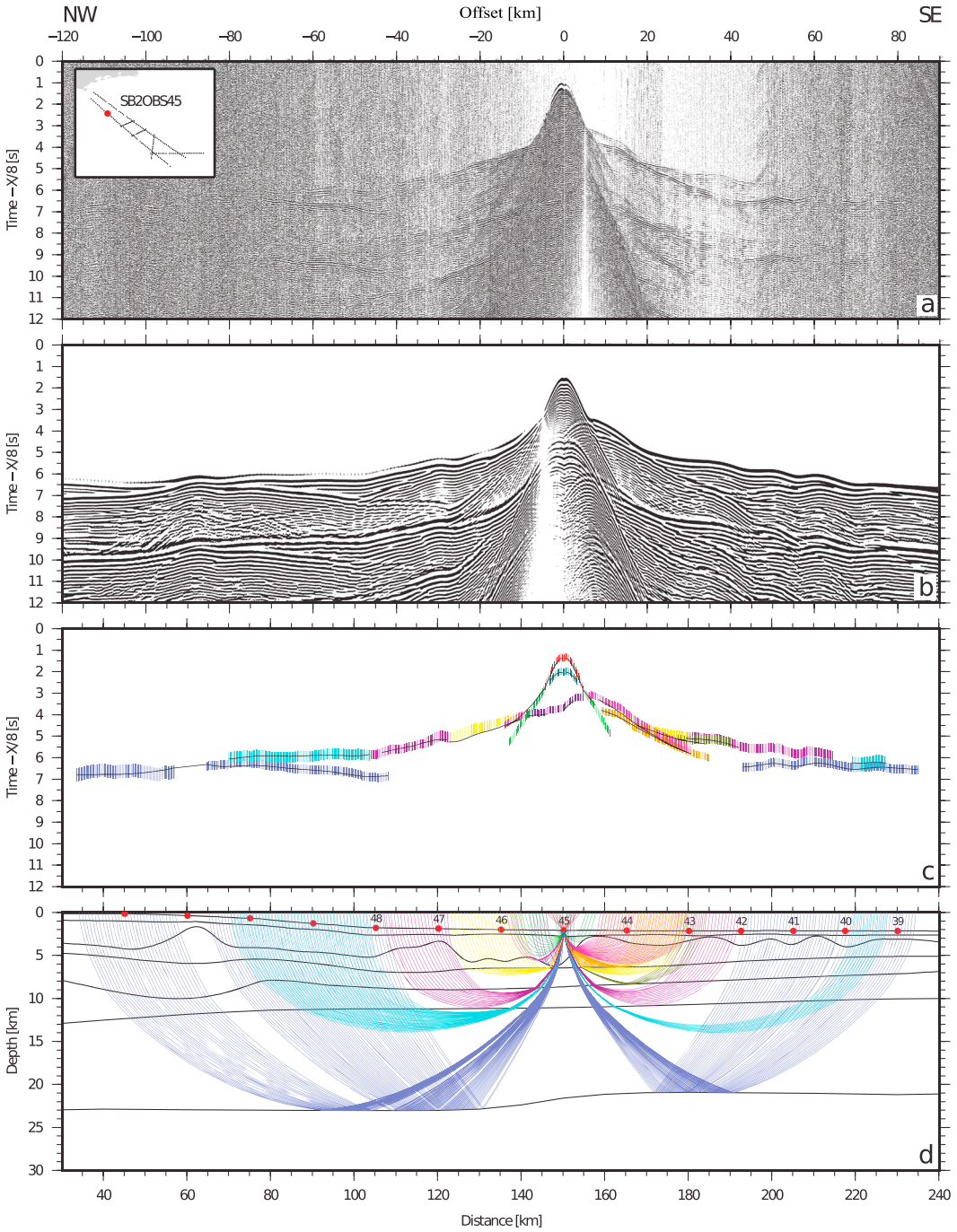

Figure 4. OBS45 on SB02 profile. Same legend and color code as Figure 2.

The salt layer sensu stricto is imaged from OBS12 to OBS43 along SB01 and from OBS55 to OBS24 along SB02. The reflection on top of the salt is characterized by a high-amplitude precritical reflected (Figures 2 and 4) phase seen at null offsets and also well constrained on the MCS data. Refracted waves in the salt appear as strong amplitude first arrivals at offsets lower than 20 km and are often seen to continue at greater offsets among secondary arrivals. Due to the presence of diapirs, some records appear highly disturbed and asymmetric but overall the apparent velocity of salt is around 4.5 km/s. In the final models, the salt layer shows velocities that vary from 4.2 to 4.7 km/s in SB01 and from 4.2 to 4.5 km/s in SB02. Its

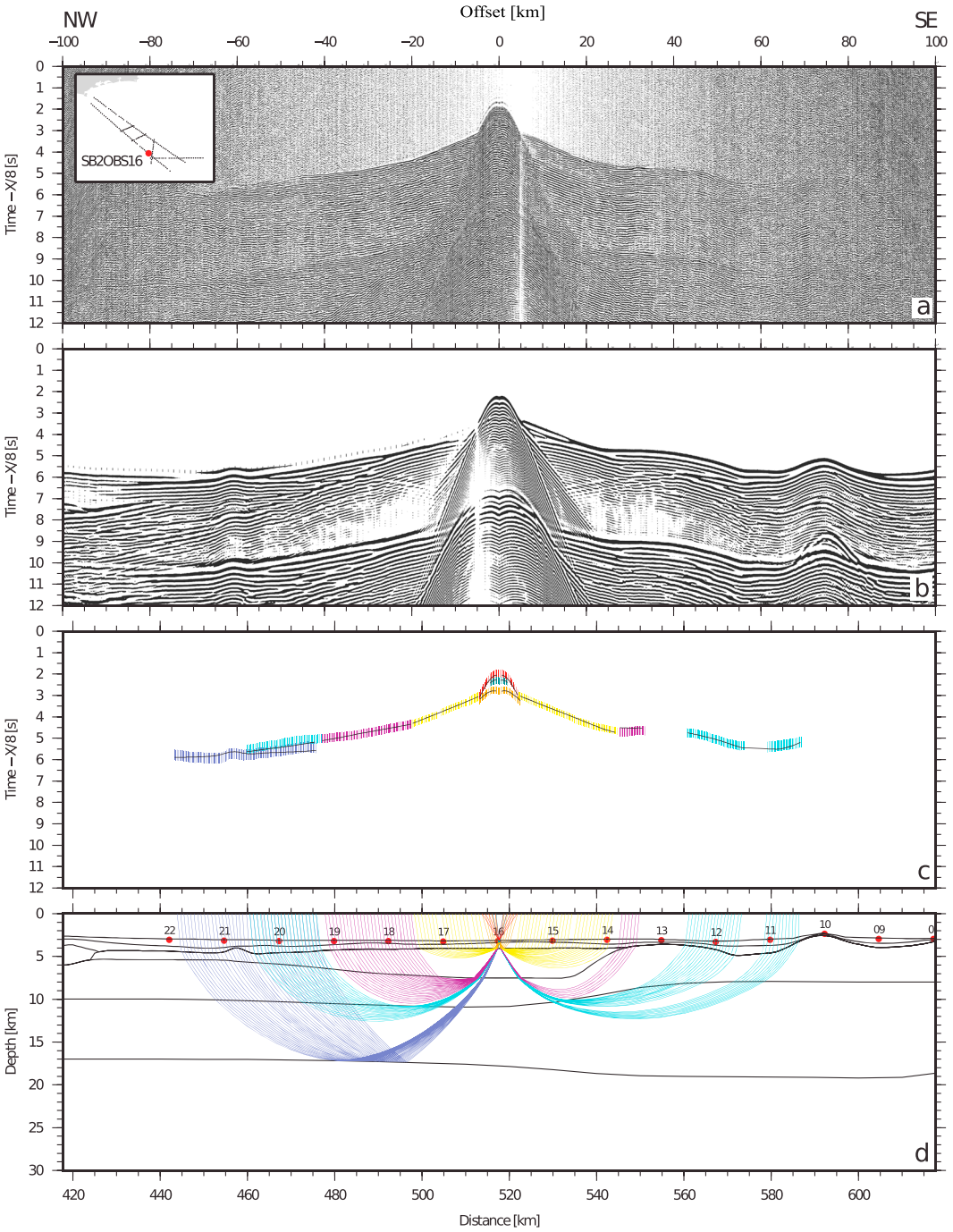

Figure 5. OBS16 on SB02 profile. Same legend and color code as Figure 2.

thickness is highly variable: from 4 km thick diapirs to almost zero between the largest one. Seaward, the salt morphology varies from small diapirs to a canopy shape and its thickness (1 to 4 km) mainly depends on basement depth variations.

In SB01, between 350 and 480 km, the salt layer is almost 5 km thick but its structure is heterogeneous and might be stratified above the basement. A few OBS indeed record reflected phases accompanied with blind zones followed by delayed refracted phases with apparent velocity close to the salt's average value, suggesting the occurrence of velocity inversions. These observations are, however, inconsistent from one

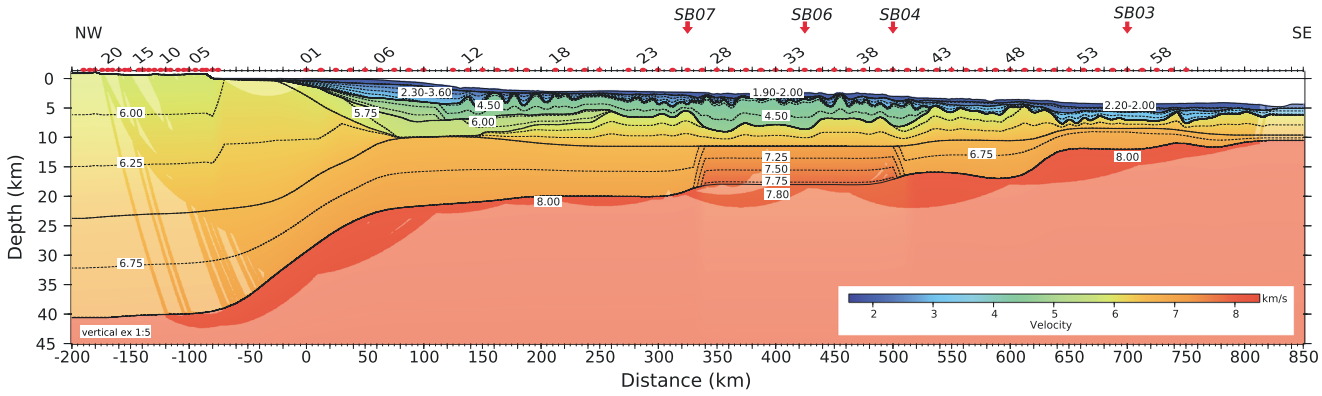

Figure 6. SB01 final velocity model based on the modeling of wide-angle seismic data. Velocities are contoured at 0.25 km/s intervals, and black lines mark layer boundaries from the modeling. Shaded areas are unconstrained by seismic rays. Red circles mark OBS positions, and arrows indicate cross-points with other SanBa profiles.

instrument to another. Keeping a single layer with salt velocities was therefore the best compromise to explain all data and keep the model simple in this area.

A presalt sedimentary layer is identified beneath the salt from the end of the continental slope to kilometer 260 on both profiles. On MCS lines (Figures S1 and S2), it is characterized by a set of strong parallel reflectors at about 5–6 s twt. Precise phase identification and estimation of the apparent velocity of presalt is difficult to perform on OBS data mostly because of the complex geometry that salt diapirs impose on first arrivals (e.g., Figure 4). On both models, the presalt layer is about 2 km thick. This average thickness associated with velocities between 5.2 and 5.7 km/s on SB01 and between 5.3 and 5.5 km/s on SB02 offers the simplest solution that allows a good fit of OBS arrivals and a good correspondence with MCS observations. In fact, we cannot exclude that velocity within the presalt layer is changing particularly toward the end of the layer on SB01 where a velocity inversion may prevail.

At last, wide-angle data imaging the deep sedimentary basin located in SB02 (420–540 km) are characterized by long almost linear first arrivals that reach offsets of 30 km with maximum apparent velocity of 5 km/s (Figure 5). The longest offsets observed for this phase are all seen on half sections recording shots from the SE, confirming the deepening of the basin toward this direction. Though the top of basement is not reflective and its position unclear on MCS data, the sharp break in apparent velocity is interpreted as the transition to crustal arrivals. This deep sedimentary basin is therefore modeled with velocities between 4.8 and 5.3 km/s on the final model. In its deepest part, it reaches 7.5 km, giving a maximum thickness of 3.5 km.

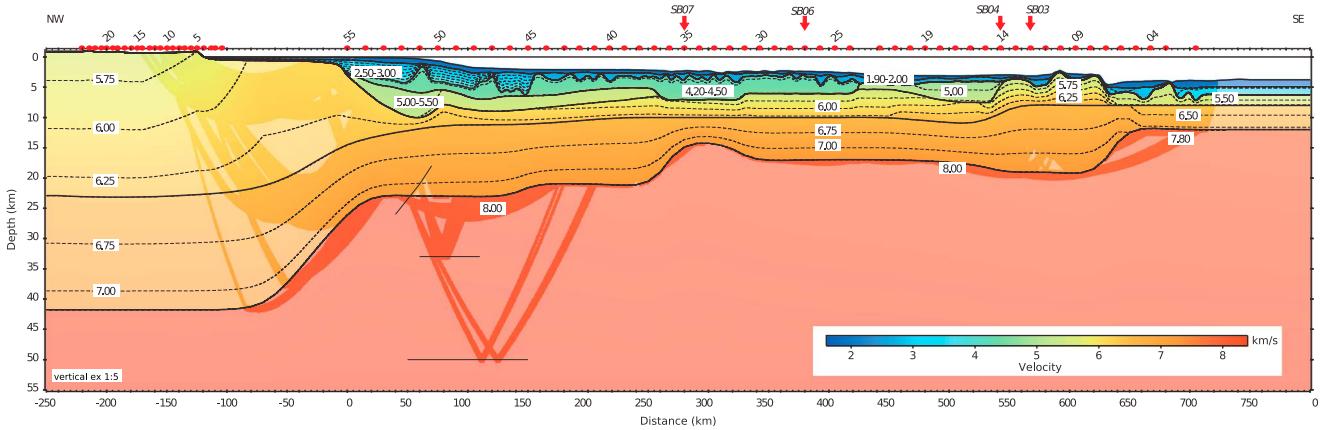

Figure 7. SB02 final velocity model based on the modeling of wide-angle seismic data. See legend of Figure 6.

4.1.3. Crustal Structure

Underlying this complex sedimentary structure, the geometry of the top of the basement is complex but well constrained everywhere, at least by one of the MCS or OBS data sets. Beneath the presalt, it slowly rises toward the SE, from 10 km beneath the slope to 6–6.5 km beneath the oceanic basin. On SB01, it remains high (6 km) until ~320 km before deepening to 8–9 km at 340 km and rising to 7 km between 440 km and 510 km (Figure 6). However, on SB02, it deepens down to 7 km just at the presalt termination (260–325 km) and then rises slightly to 6 km between 330 and 420 km (Figure 7), where the salt ends and, toward the SE, the basement is globally higher at 4–5 km depth except beneath the deep sedimentary basin identified on SB02, where it is modeled at a depth of 7.5 km. On average, the basement is at 6 km depth at the ends of the profiles but consists of many highs and lows.

Crustal arrivals on OBS data are also variable throughout the SSPS. Phase triplications between Pg, Pn, and PmP evolve from an offset of about 190 km to 150 km on land station records to about 50–100 km for a majority of OBS located over the SSPS (Figures 4 and 5) and up to 20–30 km on those located at the SE ends of the profiles (Figure 3). However, a striking difference between the two profiles exists for crustal phases imaging the central part of the SSPS. Along SB02, OBS located between 260 and 420 km have similar characteristics to those on each side, except that the cutoff of the Pg is around 50 km, suggesting thinner crust. On the other hand, along SB01, the PmP phase is clearly absent on OBS located between the crossings of SB07 and SB04. Instead, long-offset, continuous, and high-amplitude refracted phases with a 7 to 8 km/s apparent velocity can be observed (Figure 2).

On final velocity models (Figures 6 and 7), the first important feature modeled is the thinning of the continental crust on their NW ends. On SB01, the continental crust consists of two layers with velocities varying from 5.80 to 6.50 km/s and from 6.50 to 7.00 km/s, respectively. A total crustal thickness of about ~40 km to 35 km was modeled from Pn phases. Although we further controlled the continental crust thickness by gravity modeling, a velocity-thickness trade-off cannot be ruled out, since the wide-angle profile is not reversed inland. The thinning that occurs between −50 km and 100 km was modeled from PmP and Pn phases and has the shape of a necking zone. The top of the crust deepens up to 10 km, and its velocity progressively increases from 6.0 to 6.45 km/s while the Moho rises to 21 km. Similarly, on SB02, a 40 km thick continental crust was modeled with two layers which have velocities of 5.60–6.35 km/s and 6.50–7.10 km/s, respectively. The necking zone, located from −50 to 100 km, leads to a 13 km thick crust with an upper velocity increasing to 6.2 km/s and a Moho depth at 23 km. On both profiles, the velocity at the bottom of the crust remains constant across the necking zone.

A second zone of crustal thinning is imaged at the center of the models, where a deeper basement is also observed. The velocity structure is, however, very different between SB01 and SB02. On SB01, from 340 to 500 km, below a 3–5 km thick, high-velocity (6.0–6.5 km/s), upper basement layer, a second 6.5 km thick layer with velocities increasing from 7.0 to 7.8 km/s from top to bottom is required in order to model the long-offset and high-amplitude refracted phases described previously. By contrast, on SB02 (250–350 km), the Moho rises to a minimum depth of 14.5 km, but the crustal structure and velocities remain similar to those modeled on each side, with upper (5.6 to 6.3 km/s) and lower (6.5 to 7.1 km/s) layers between 7 and 10 km thick.

Surrounding this central region, the crust on both SB01 and SB02 has a similar velocity structure. The upper crust velocities are lower than 6 km/s, varying between 5.3 and 5.8 km/s, while the lower crust velocity does not exceed 7.2 km/s. The total crustal thickness varies between 10 and 17 km. Only the SE ends of the two models are marked by a prominent and abrupt decrease in Moho depth and crustal thickness. In SB01, the crust consists of two crustal layers (6.0–6.5 and 6.7–7.0 km/s). The Moho at 11–12 km corresponds to the noncontinuous reflectors observed on the MCS profile (blue arrows on Figure S1). Along SB02, the thinning marks the crossing of the São Paulo Ridge and Fracture Zone and the presence of oceanic crust. It is 6 km thick and made of two layers (5.3–5.7 and 6.3–6.8 km/s), with a Moho at 12 km depth.

4.1.4. Lithospheric Mantle Structure

The base of the two models consists of a lithospheric mantle layer with a constant upper velocity of 8.0 km/s that allows a good fit of the Pn arrival times observed on OBS records. The only exception occurs in the central part of SB01 where the velocity at the top of this layer starts at 7.8 km/s. No velocity step is

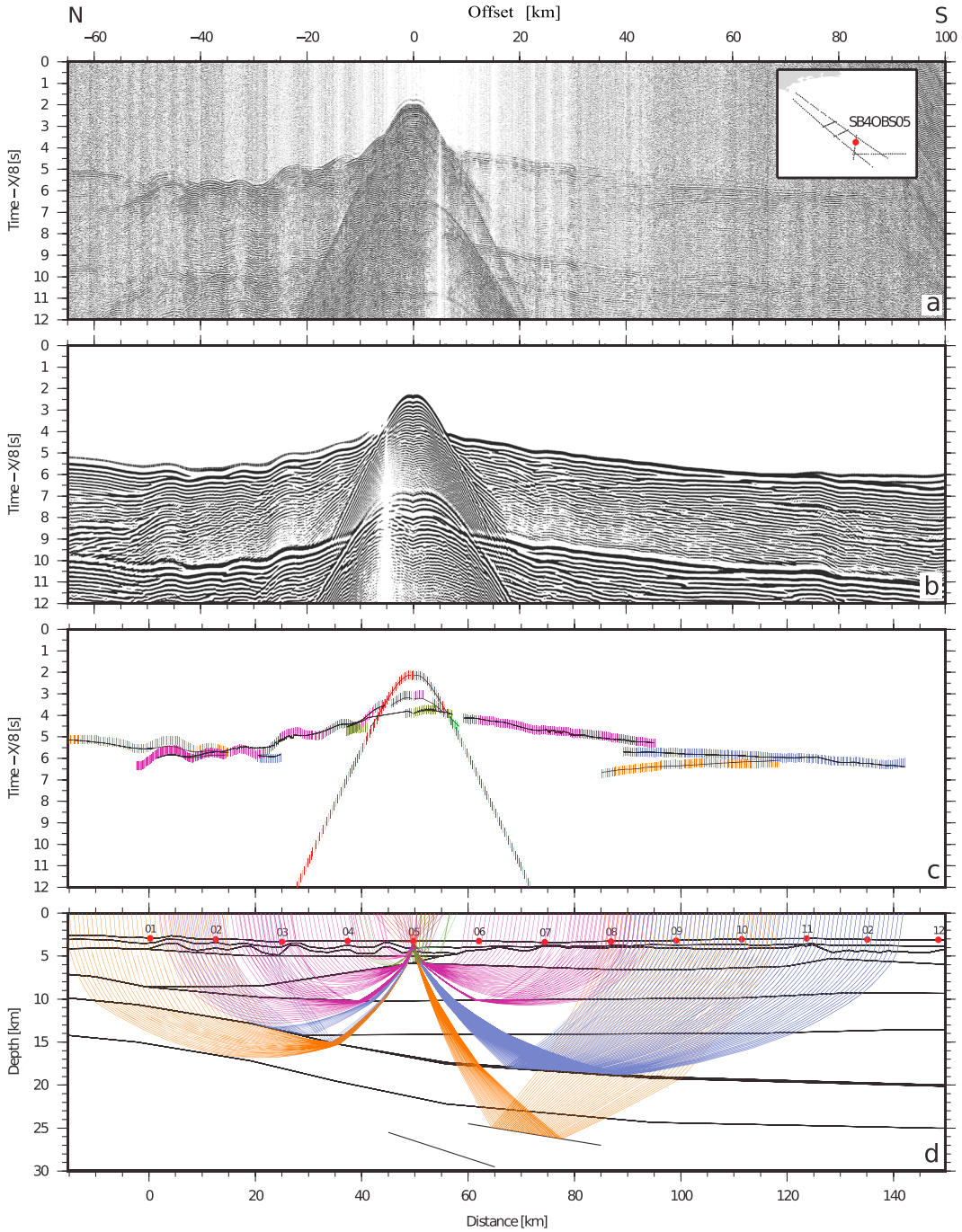

Figure 8. OBS05 on SB04 profile. Same legend and color code as Figure 2.

required here without any evidence of a reflection from the Moho on OBS data. A few late secondary arrivals are observed on some OBS located over SB02. We interpreted these arrivals as reflected phases from the lithospheric mantle (Figure 3). These can be explained by the presence of reflective interfaces within the mantle, but with the lack of constraints on the lithospheric mantle structure, their depth and position (50–150 km) are highly uncertain.

4.2. Profile SB04

SB04 is the N-S profile crossing SB01 and SB02 and terminating at the São Paulo Ridge (Figure 1). On the MCS line (Figure S3), salt domes are present in the first 50 km, while a sedimentary basin covers the rest of the line.

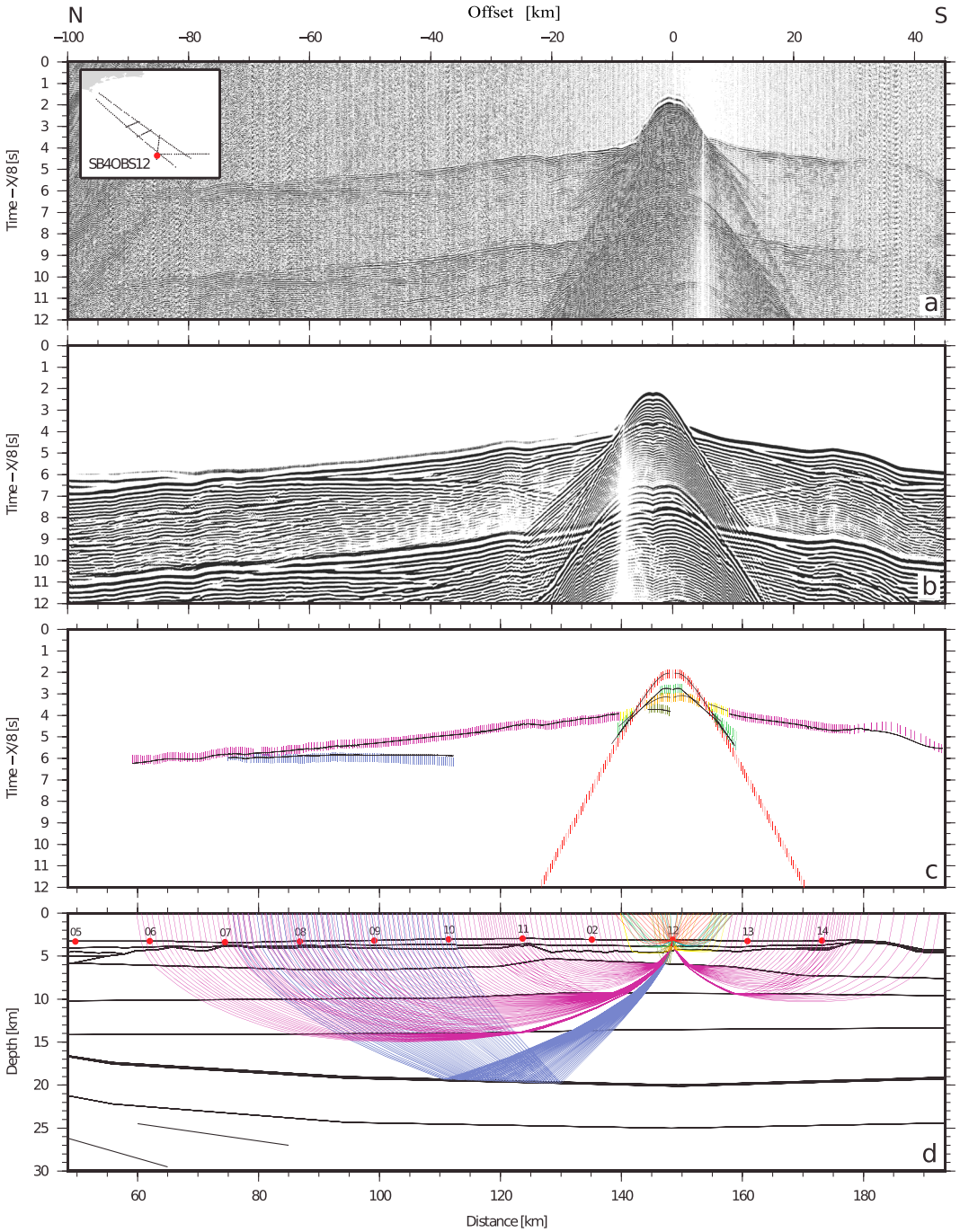

Figure 9. OBS12 on SB04 profile. Same legend and color code as Figure 2.

This basin shows an internal prominent and waving reflector around 5 s twt sealing a succession of later events observed up to 6 s twt. These reflectors reveal the northward extension of the deep sedimentary basin described in SB02.

4.2.1. Uppermost Sedimentary Structure

In the near-offset range (up to ~5–10 km) of most OBS data recorded along SB04, two secondary refracted arrivals are visible with apparent velocities of 2.0 and 2.5 km/s, corresponding to the upper sedimentary cover also described along the two main profiles (Figures 8 and 9). Reflected phases at the interfaces of these sediments are again well visible inside the water wave arrivals' cone and have travel times consistent with the main sedimentary reflectors seen on the MCS line (Figure S3).

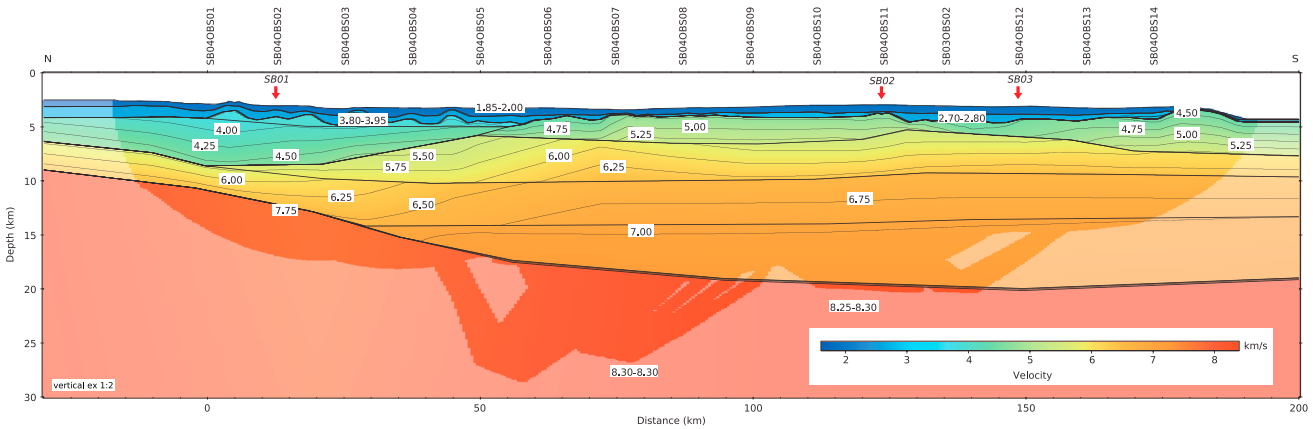

Figure 10. SB04 final velocity model based on the modeling of wide-angle seismic data. See legend of Figure 6.

The SB04 final model (Figure 10) consists therefore of two uppermost sedimentary layers, with velocities of 1.85–2.0 km/s and 2.55–2.8 km/s. These sedimentary layers are overall less than 2 km thick, they thin to about half a kilometer in the central part of the profile (~80 km), and their thickness is highly variable between salt diapirs.

4.2.2. Deep Sedimentary Structure

At offsets less than ~20 km, first arrivals recorded in the five northern OBS (OBS01–OBS05) correspond to refracted waves in the salt. Their apparent velocities span from ~3.5 km/s to ~4.5 km/s due to the presence of diapirs (Figure 8). This geometry is, however, well constrained by both precritical reflections on OBS data and a strong reflector present on MCS (Figure S3).

The next 10 OBS (OBS06–OBS14) record almost linear and strong first arrivals with varying apparent velocities (4 to 5 km/s) in the offset range from 10 to 20 km (Figure 9). The top of this layer consists of the very bright and continuous reflector at 5 s twt on MCS (Figure S3) and a strong reflection phase within the water cone of OBS sections (Figure 9). In contrast, as for SB02, its base is not well imaged by the MCS data but can be constrained nevertheless by a break of first arrivals' apparent velocity and sparse near-offset and wide-angle reflected phases (Figure 9). A decrease in the offset of the crossover point with deeper phases reveals a thinning of this basin south of the crossing of SB04 with SB02, where it attains its maximum thickness.

In the final velocity model (Figure 10), the salt layer presents upper velocities ranging from 3.5 to 4.1 km/s and a bottom velocity of ~4.8 km/s. The base of the layer is constrained by reflections identified on four OBS records that require its pronounced southward shallowing from ~8.5 km to ~5 km, over its last ~20 km. Further south, the deep sedimentary basin has a velocity of ~4.7 km/s at ~4 km depth that increases up to ~5.3 km/s at ~6.5 km depth. Approaching the Florianópolis Fracture Zone (FFZ), this basin gets thicker (3–3.5 km) and its base deeper (7 km). Its surface is more rugged with velocities decreasing to ~4.3–4.5 km/s while its bottom velocity reaches 5.5 km/s.

4.2.3. Crustal and Upper Mantle Structure

The Pg phase is identified as a first arrival in large-offset bands for most of the OBS seismic record sections. In the first 50 km of the profile, its apparent velocity is affected by the salt topography but, from 50 km southward, it clearly increases with offset, from ~5.7 km/s to ~7 km/s (Figures 8 and 9). The offset extent of the Pg is highly variable from just ~5 km in the north of the profile (OBS02), increasing up to ~30 km on OBS05 (Figure 8), to at least ~60 km over the remaining OBS (e.g., Figure 9). This observation indicates an important northward crustal thinning that corroborates observations made on the two main profiles. On OBS06 to OBS14, the PmP is a remarkably strong and long (it runs over 70 km) precritical phase, while it is absent from the northernmost OBS records as in SB01.

Pn phases can be identified as very fast (more than 8 km/s) first arrivals in the six northern OBS (OBS01–OBS06) where it becomes a first arrival at offsets of only ~20–40 km, indicative of extremely thin crust. We did not identify Pn phases on the other records. Three OBS (OBS04, OBS05, and OBS09) also show strong reflections interpreted to originate from the mantle (Figure 8).

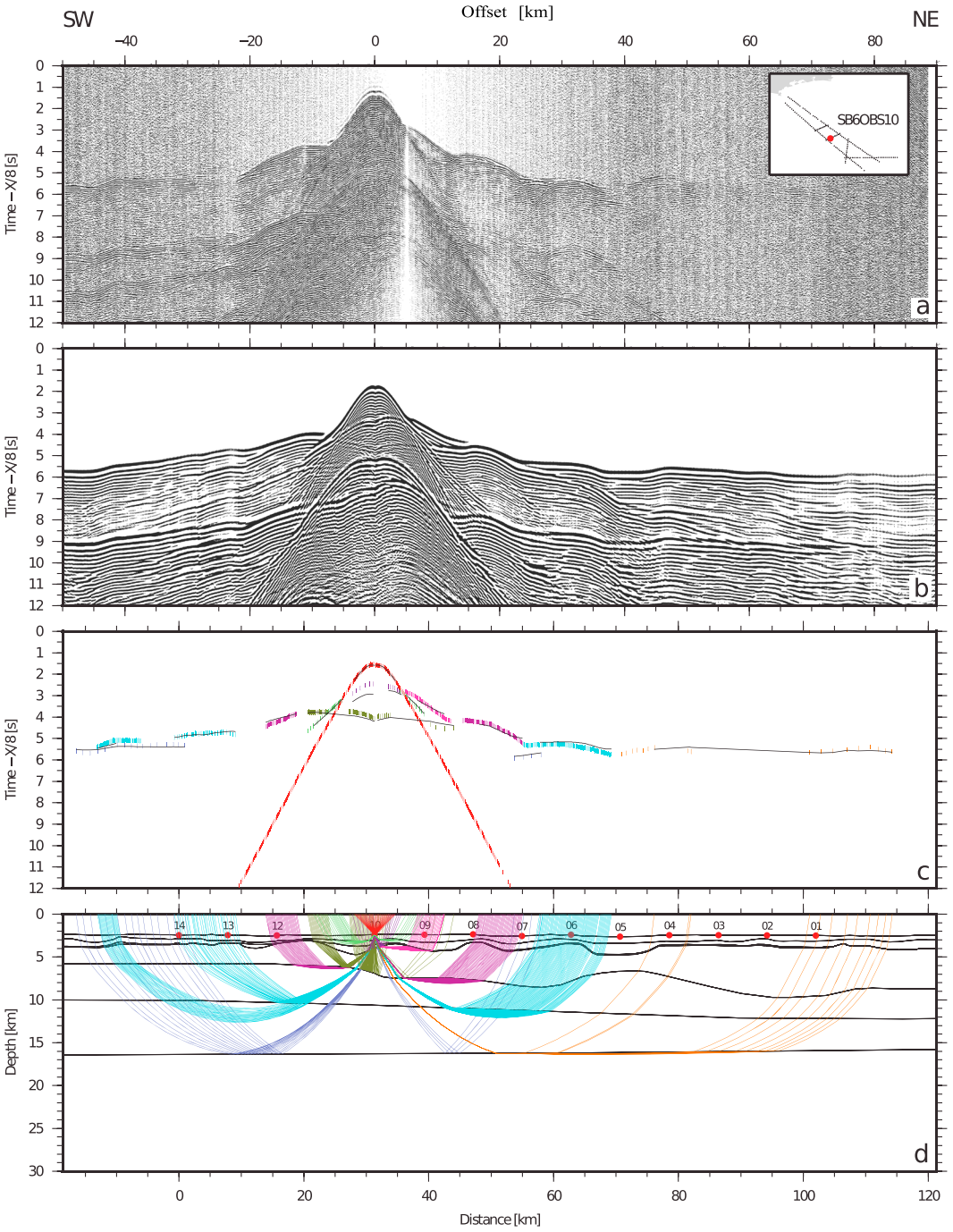

Figure 11. OBS10 on SB06 profile. Same legend and color code as Figure 2.

The final model indicates mantle-like velocities of ~7.7 km/s at only 11 km beneath the first OBS (0 to 20 km). The extremely thin crust (2–3 km thick) present here has velocities that range from 5.6–5.7 km/s in its upper part to 6.4–6.9 km/s at its base. Further south, the Moho deepens with an ~8° slope to ~17.5–20 km. There, velocities in the upper crust are between 5.5 and 6.0 km/s and increase with depth to a maximum of ~7.2 km/s.

4.3. Profile SB06

SB06 strikes perpendicularly to SB01 and SB02 (Figure 1). The MCS profile (Figure S4) shows an upper sedimentary cover affected by salt domes except in the 40 km at the NE extremity of the line where the salt

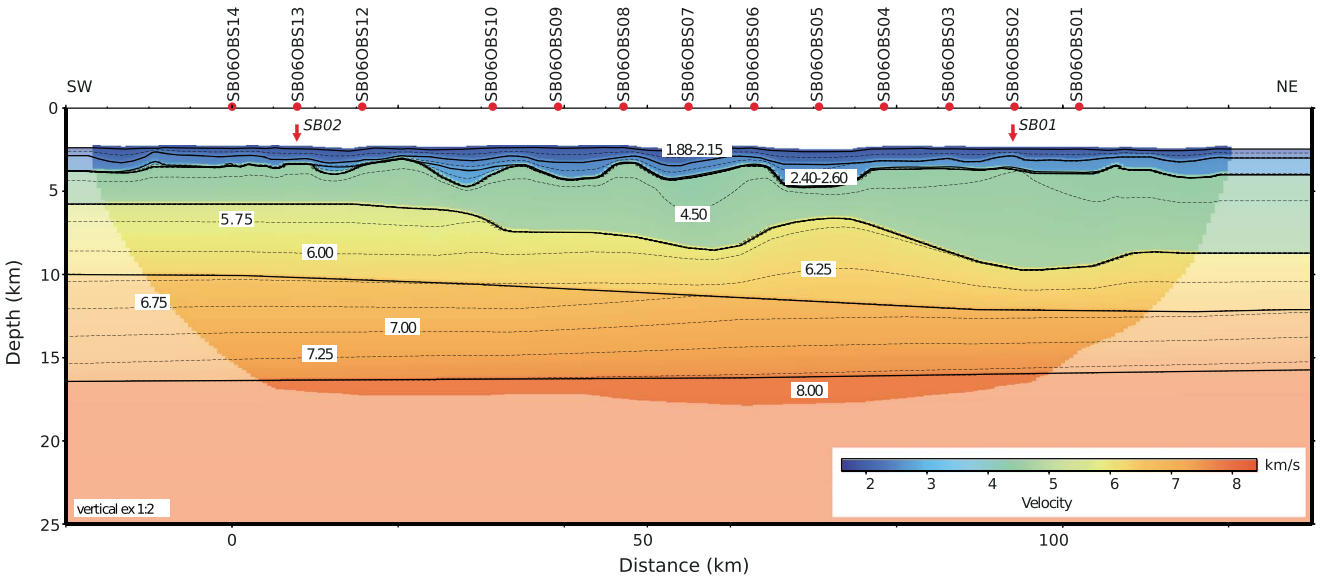

Figure 12. SB06 final velocity model based on the modeling of wide-angle seismic data. See legend of Figure 6.

surface flattens. Though noncontinuous, the basement is clearly seen and deepens from 5 s at the crossing with SB02 (SW) to ~7 s at the crossing with SB01 (NE).

4.3.1. Sedimentary Structure

As already noticed in this area along the two main profiles, the salt topography makes OBS sections asymmetric along SB06. At short offsets, refracted phases in this salt layer appear as first arrivals while uppermost sedimentary phases come as secondary arrivals. Apparent velocities are again clearly lower than 3 km/s in uppermost sediments and approximately 4.5 km/s in salt. Associated near-offset reflected phases are visible within the water cone; the top of the salt is a strong reflector on MCS data, generating also particularly high amplitude reflected phases on OBS data (Figure 11).

The SB06 final velocity model (Figure 12) consists of a continuous uppermost sedimentary structure with velocities between 1.9 and 2.6 km/s. Its thickness varies between 1 and 2 km according to the salt topography. Between larger diapirs, uppermost sediments can reach a maximum thickness of 2.5 km, and their velocity increases to 2.8 km/s (e.g., beneath OBS10 at 25 km). Deeper, the salt layer has upper velocities varying between 4.3 and 4.5 km/s. They increase to 4.7 km/s at its base. It is only 2 km thick in the WSW of the model and thickens progressively toward the ESE to reach 5–6 km.

4.3.2. Crustal Structure

The eastward dipping trend of the basement observed on the MCS data (Figure S4) is confirmed on OBS data. From OBS14 to OBS12, the crossover between refracted phases in the salt and upper crust is at an offset of ~15 km, while for the sections OBS10 to OBS06, this occurs at offsets close to 20 km (Figure 11). On the last five sections (OBS05 to OBS01), this crossover appears back at an offset of about 15 km to return progressively to 20 km, suggesting a basement high. Pg arrivals are observed on all OBS sections, but only those recorded over the western half of the profile show clear PmP reflections (see difference between E and W sides of the section shown in Figure 12). Upper mantle Pn events are of weak amplitude and recorded from OBS04 through OBS13, with the exception of OBS10.

In the final model (Figure 12), the top of the acoustic basement dips eastward from 6 km to approximately 9 km. As suggested by OBS data, this trend is perturbed by two topographic features: a step at 30 km where the basement depth suddenly increases from 6 km to 7 km and a remarkable high between 60 and 90 km where it rises from 8.5 km to 6.6 km and then goes down to 9.7 km before returning to 8.7 km beneath OBS01. Two layers were used to model refracted phases in the crust while a few reflections allow constraining of their interface (from 0 to 10 km and 60 to 90 km). There is also an overall increase of velocity toward the NE. While in the SW velocities range from 5.6 to 6.2 km/s in the upper layer and 6.5 to 7.5 km/s in the lower layer, in the NE they rise to 6.0–6.5 km/s and 6.9–7.6 km/s, respectively. This lateral velocity gradient coincides with

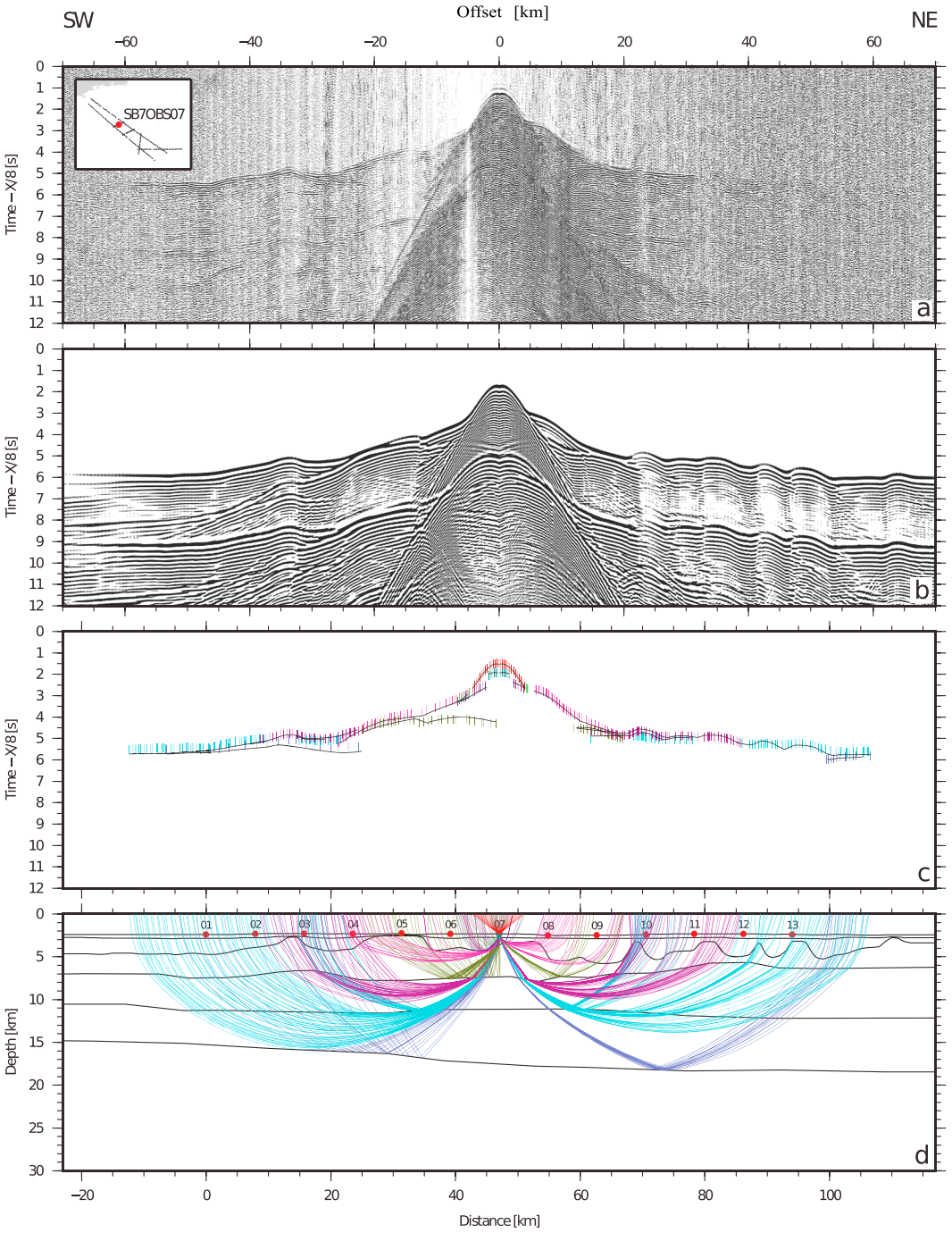

Figure 13. OBS07 on SB07 profile. Same legend and color code as Figure 2.

a progressive thinning of the two layers from about 11 to 7 km. Finally, the bottom layer of the model consists of an upper velocity of 7.8 km/s. Overall, the modeling of SB06 confirms, after SB01 and SB02, that the central part of the SSPS is highly heterogeneous.

4.4. Profile SB07

SB07 also runs perpendicularly to SB01 and SB02 (Figure 1). Salt is present across the entire MCS profile (Figure S5). Diapirs appear fewer but larger on the western half of the line than on its eastern half. The basement is a particularly strong and quite continuous reflector between 5 s twt and 6 s twt, rising clearly at about 70–80 km and remaining high in the NE end of the profile.

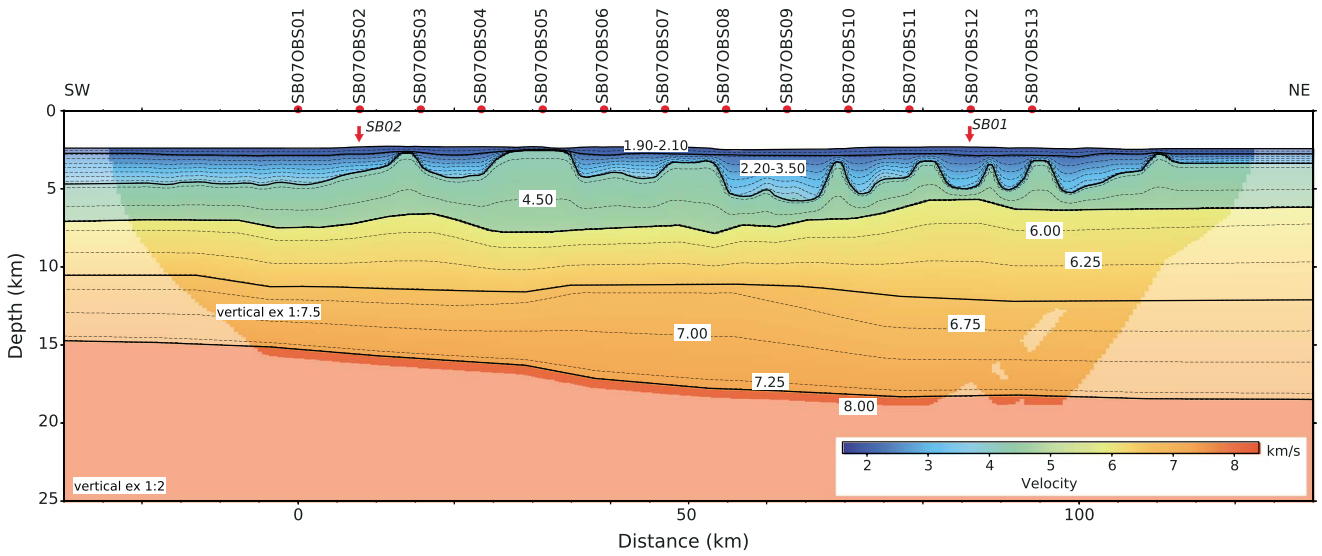

Figure 14. SB07 final velocity model based on the modeling of wide-angle seismic data. See legend of Figure 6.

4.4.1. Seismic Data

Every OBS section of profile SB07 shows again refracted arrivals heavily disturbed by salt diapirs. High amplitudes mark the triplication between salt and crustal phases (Figure 13). Confirming the deepening of the basement toward the SW, triplications occur at increasing offsets, from 10 km at the crossing with SB01 to 20 km at the crossing with SB02. On most sections, Pg arrivals are clearly identifiable but PmP and Pn phases are mostly weak if identifiable.

4.4.2. Velocity Model

The SB07 final velocity model (Figure 14) comprises two uppermost sedimentary layers, a salt layer, two crustal layers, and a lithospheric mantle layer. The two uppermost sedimentary layers are characterized by low seismic velocities of 1.9–2.1 km/s and 2.2–3.5 km/s and highly variable thicknesses, the highest velocities being found where sediments are the thickest between diapirs. The underlying salt layer shows velocities between 4.2 and 4.7 km/s and forms domes as much as 5 km thick. Salt thins drastically to a few hundred meters at the crossing with SB01 because the basement rises from 7.5 km to a depth of 6 km. Crustal thickness increases from about 8 km (Moho at 15–16 km) in the southwestern end of the profile (SB02) to 13 km (Moho at 18–19 km) in its northeastern end (SB01). It comprises two layers of velocities respectively between 5.9–6.5 km/s and 6.6–7.3 km/s. These velocities remain constant throughout the line as lithospheric mantle velocity which is found to be 8.0 km/s.

5. Discussion

5.1. New Proposed Segmentation of the SSPS

Based on the velocity models described above, a new segmentation of the SSPS is presented in Figures 15 and 16. This subdivision is coherent with the observation of the gravity and magnetic grids (Figure 17). Each domain's characteristics are presented here, and a discussion on their nature follows.

1. In the NW, the onshore extensions of SB01 and SB02 allow the identification of an unthinned continental crust domain (Domain CC) and a necking zone domain (Domain N). The unthinned crust is ~35–40 km thick with velocities between 5.6 and 7.0 km/s. In Domain N, the Moho rises to less than 25 km and the basement surface deepens to 10 km while its velocity increases to 6.4 km/s. The necking zone is very narrow, with an extension of less than 100 km. It also shows very thin, SW-NE structured magnetic lineaments and strong SW-NE positive gravity anomalies.
2. Further SE, Domain A consists of a thin crust. It is characterized by some salt and presalt overlaying an 11 to 15 km thick crust with seismic velocities between 6.0 and 7.0 km/s. The top of the crust and the Moho rise slowly toward the SE with a slight increase in crustal thickness and decrease in upper crust velocity. We define a subdomain A' at the southeastern end of Domain A where presalt is absent but minor

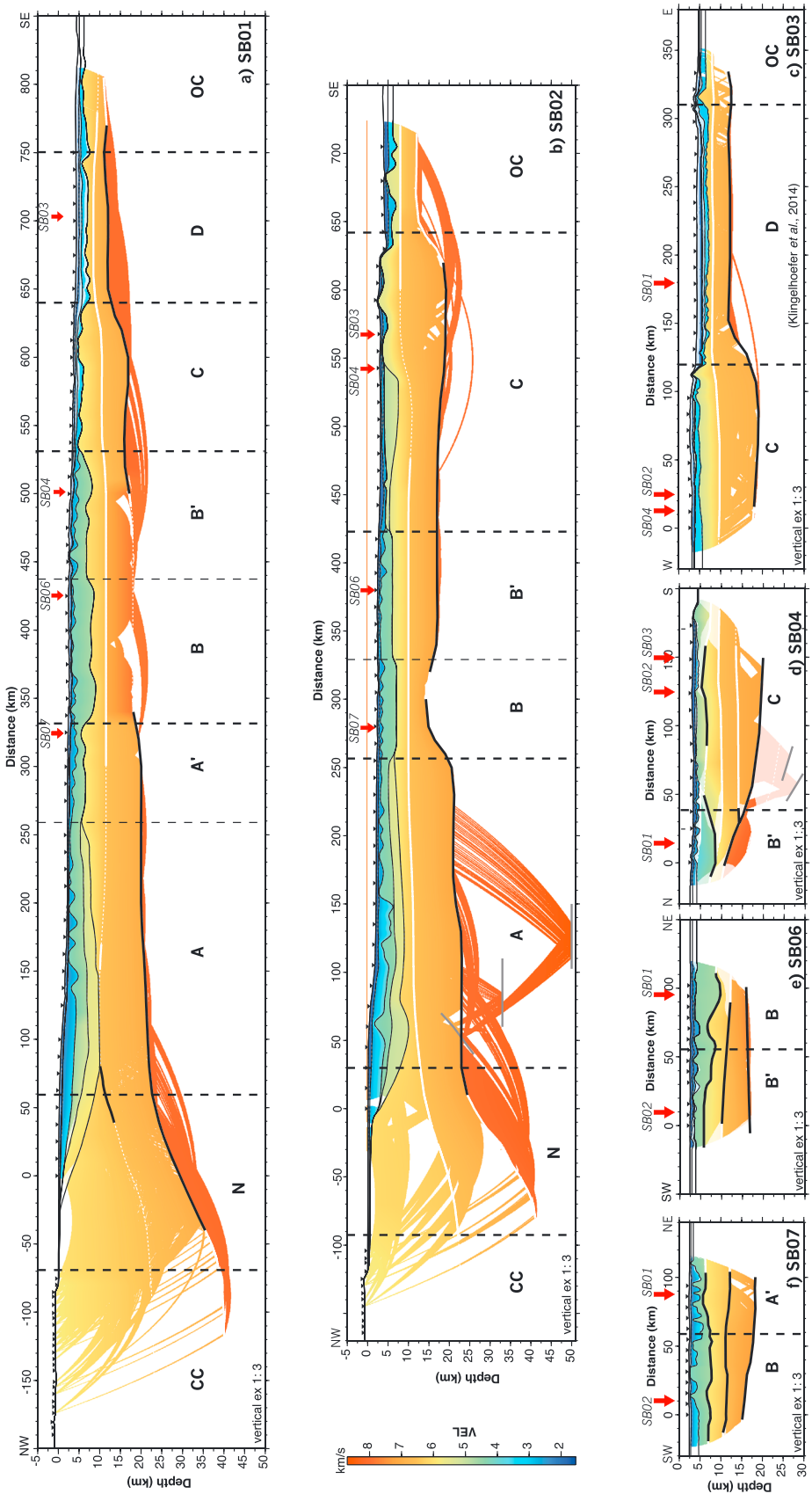

Figure 15. Synthesis of results from the SanBa seismic experiment. Velocity models for (a) SB01, (b) SB02, (c) SB03, (d) SB04, (e) SB06, and (f) SB07 are all divided according to the new proposed segmentation of the SSPS. Only resolved regions in models are shown; unresolved regions appear in white. See Figures S7a–S7e for details on resolution tests. Upper interfaces displayed as thin black lines are geological interface constrained by MCS data. Thick black lines indicate deep geological interface constrained by wide-angle reflections. Dashed and continuous white lines differentiate unresolved from resolved interfaces needed for modeling purposes.

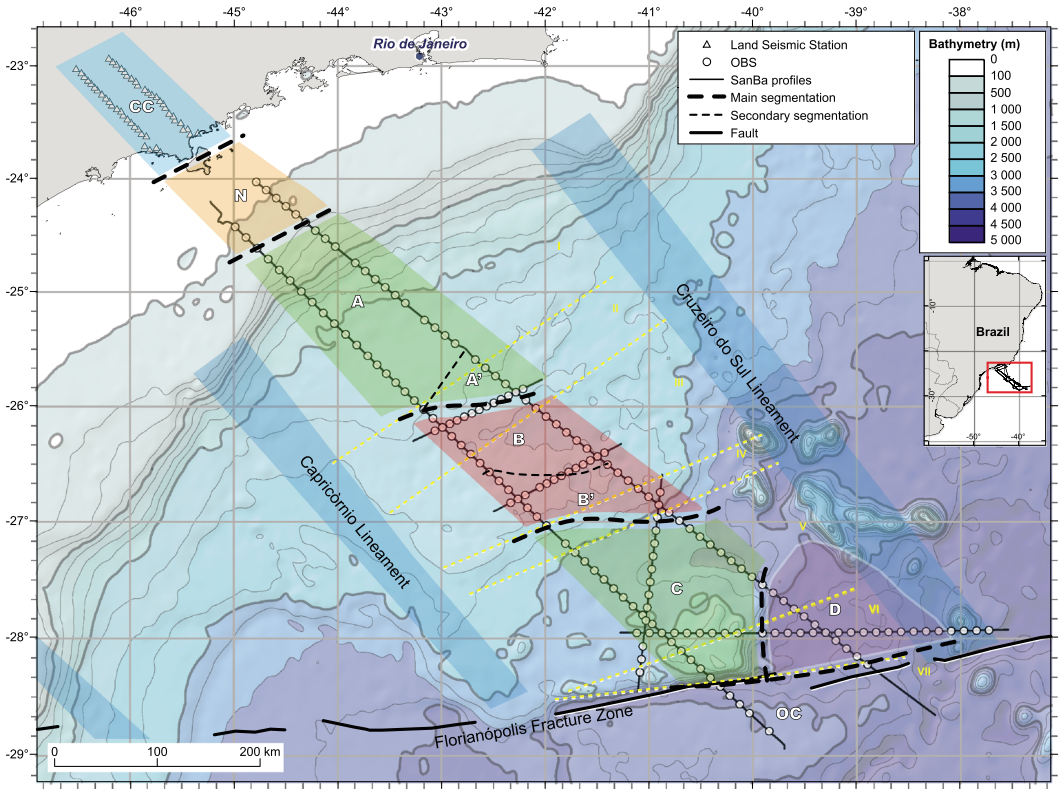

Figure 16. New segmentation of the SSPS over predicted bathymetry [*Smith and Sandwell*, 1997]. New domains are delimited by colored polygons separated by thick dotted black lines (CC: continental crust, N: necking zone, OC: oceanic crust, see discussion for nature of Domains A to D) and thin dotted black lines between subdomains A-A′ and B-B′. Thin black lines are SanBa wide-angle seismic profiles; white circle and triangles are OBS and land seismic stations; yellow dashed lines indicate the segments previously defined by *Moulin et al.* [2012].

changes on the crustal structure are observed: the basement is at only 6 km depth with a velocity as low as 5.8 km/s, and the crust is 15 km thick. This subdomain has a triangular shape because it is about 70 km large on SB01 but does not exist on SB02. Domain A-A′ corresponds to a low anomaly and a high anomaly on the gravity and magnetic maps, respectively.

3. In the center of the SSPS, Domain B is a region of very thin crust that extends as far as the oceanward limit of the salt. At the boundary with Domain A, the salt changes to a canopy-style morphology and the basement deepens by 1 to 2 km. It is the domain that shows the most heterogeneous crustal structure. Its whole northeastern part (SB01) has a crust 2.5 to 5 km thick with velocities between 6.0 and 6.5 km/s overlying a layer of anomalous velocity (7.0–7.8 km/s) without any reflection from the Moho. By contrast, its southwestern part (SB02) is characterized by velocities similar to that in Domain A or C though with a much thinner crust (between 7–8 km and 11 km thick). Domain B is an area of low magnetic and high gravity anomalies. The gravity map exhibits stronger N80-aligned gravity anomalies along the boundaries of Domain B with Domains A and C. This observation may be connected with the sharp changes in crustal thickness and Moho depth. A subdomain B′ is defined on the SE half of Domain B where the top of the basement slightly rises and/or the Moho deepens compared to its northeastern half.
4. Domain C shows a pattern similar to Domain A with high positive magnetic anomalies and low gravity anomalies. It also depicts a crustal structure close to Domain A except it has a lower upper crust velocity (5.2 km/s). It is 11 to 17 km thick with a velocity of 6.9 km/s above the Moho. Salt is absent in this domain, but its southern part is characterized by a 3.5 km thick deep sedimentary basin that bounds the São Paulo Ridge and FFZ.
5. Domain D presents a 5 km thick atypical crust made of a thin upper layer (1–1.5 km) that presents velocities varying from 6.0–6.3 to 6.5 km/s and a 3–4 km thick lower layer with velocities of 6.7–7.0 km/s.

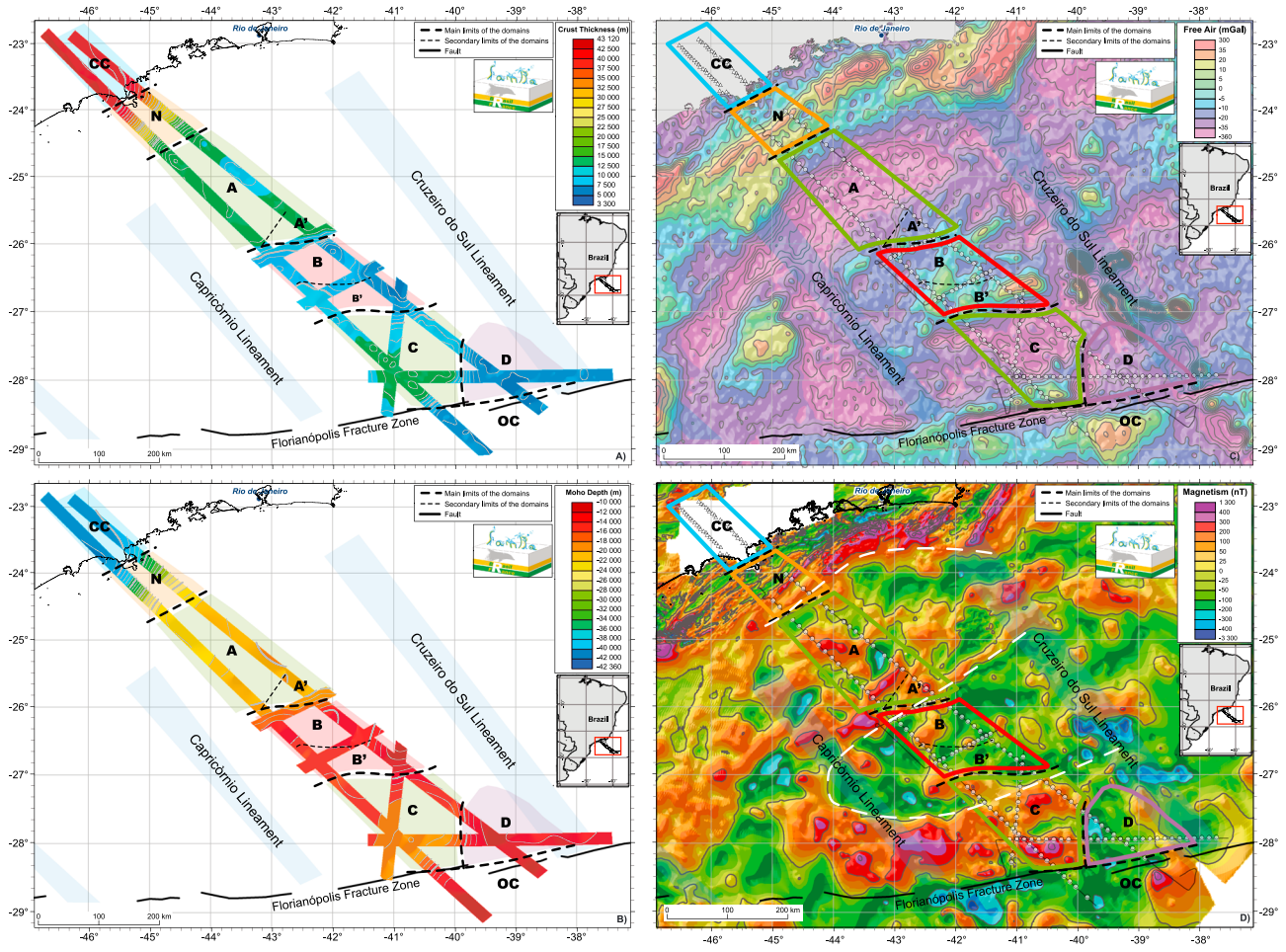

Figure 17. Maps of the SSPS showing (a) crustal thickness, (b) Moho depth, (c) satellite-derived free-air gravity anomaly [*Sandwell and Smith*, 2009], and (d) magnetic anomaly reduced to the pole (Petrobras internal database based on EMAG2 [*Maus et al*., 2009]). The new segmentation of the SSPS appears in contour-colored polygons and/or separated by thick dotted black lines and thin dotted black lines between subdomains A-A' and B-B' (CC: continental crust, N: necking zone, OC: oceanic crust, see text for nature of Domains A to D). Thin black lines are SanBa wide-angle seismic profiles; white circle and triangles are OBS and land seismic stations. On Figure 17d, the thick dotted white lines separate areas with predominantly negative magnetic anomalies from areas with predominantly positive magnetic anomalies.

Located to the southeastern part of the SSPS, South of the Jean Charcot Seamounts where a strong step in bathymetry, a low gravity, and calm magnetic and areas exit, this domain has a triangular shape. Also imaged at the center of SB03, the nature of Domain D is discussed in the recent article by *Klingelhoefer et al*. [2014] who infer the presence of proto-oceanic crust in this area based on the atypical velocity structure of the basement.

6. Finally, oceanic crust located at the SE extremity of the experiment (Domain OC) is barely imaged at the termination of SB01, but its velocity structure is better constrained at the end of SB02.

This segmentation shows a global v-shaped structure. The limits between domains are parallel to the coast in the northern part of the SSPS while they are mainly N85° in its central and southern parts. These orientations are different from the rest of the central segment of the South Atlantic and confirm that the opening direction of the SSPS was oblique to the general opening motions of the South American and African plates [*Cobbold et al*., 2001; *Meisling et al*., 2001; *Moulin et al*., 2012; *Heine et al*., 2013]. It is also worth to note that the central and southern limits between domains are not exactly perpendicular to the lineaments (Cruzeiro do Sul and Capricórnio, Figure 1) and transfer zones [*Cobbold et al*., 2001; *Meisling et al*., 2001]. Instead, they trend parallel to the Florianópolis Fracture Zone and the general opening motions of the South American and African plates. This may imply that, despite its main oblique opening direction, the South America/Africa global movement had an influence on the SSPS structures.

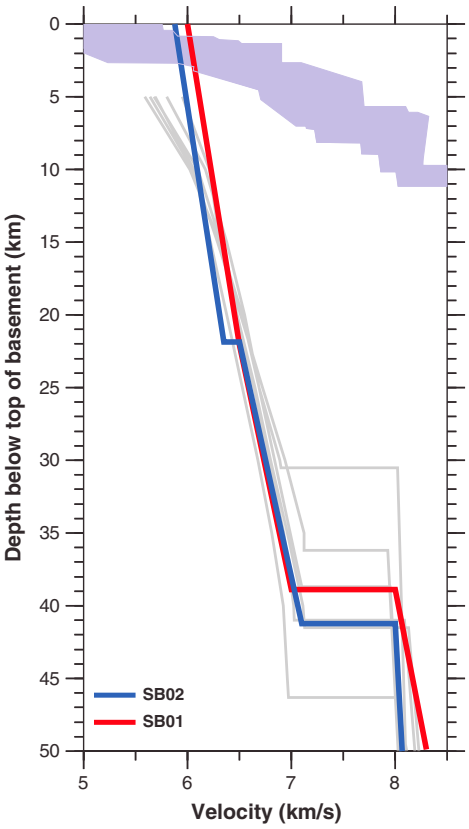

Figure 18. One-dimensional velocity-depth below basement (VZ) profiles from SB01 (red line) (−100 km) and SB02 (blue line) (−120 km). The blue shaded area bounds a compilation of velocity profiles for the Atlantic oceanic crust [*White et al.*, 1992] while gray profiles correspond to the average velocity profiles of the five tectonic provinces defined by *Christensen and Mooney* [1995] plus their reference profile for continental crust.

5.2. Crustal Structure of the Continental Crust: Domain CC

Figure 18 shows a comparison of 1-D velocity-depth profiles from both profiles SB01 and SB02 with a worldwide compilation of unthinned continental crust [*Christensen and Mooney*, 1995]. All these profiles display clear similarities in both their velocity range and gradient as well as absence of, or only a small, velocity step at the transition between upper and lower crustal layers (around 22 km depth). Although it was necessary for modeling purposes to include two crustal layers of different velocity gradient, the existence and exact position of their common boundary should be considered as uncertain. Indeed, to accurately constrain the crustal thickness at the onshore/offshore limit, on-land shots would have been needed.

The crust in the continental area onshore Brazil has been found in a recent compilation of seismic data [*Assumpção et al.*, 2013a] with an average thickness of 39 ± 5 km. The continental crust is the thickest in Southern Brazil, precisely in the Paraná Basin where good quality receiver function measurements indicate values of 42 ± 4 km [*Assumpção et al.*, 2002, 2013b]. Closer to the coast of SE Brazil, the crust is slightly thinner than average. An onshore refraction seismic experiment made in the Serra do Mar near Ubatuba (east of São Paulo) measured a 36.2 km (±2.6 km) thick crust [*Bassini*, 1986, in *Cobbold et al.*, 2001]. These values are globally in the range of what is found along the two main SanBa profiles though they suggest a thicker crust beneath the coastline than previous studies. Overall, these results imply that the crust imaged in Domain CC is not thinned and the thinning process for the SSPS basin system begins offshoreward.

5.3. Crustal Structure and Geometry of the Continental Crust Necking Zone: Domain N

Domain N of the SSPS depicts SW-NE well-structured magnetic anomalies (Figure 17d) and is the place where the continental crust thins from ~35–40 km to less than 15 km. On 1-D velocity-depth profiles (Figure 19), the thickness of the upper crustal layer decreases drastically while its upper velocity increases. This can be explained by a progressive removal of the upper crust (or exhumation of middle/lower crust) or by the increasing mass of a thickening sedimentary cover (i.e., reducing the porosity and increasing the density of the crust) or by a combination of both. In the lower layer, the top and bottom velocities do not change but its thickness also decreases. Overall velocity-depth profiles have a continental crust signature with a global increase in the mean velocity and the velocity gradient as the crust becomes thinner.

The necking is very narrow and occurs over a distance of less than a hundred kilometers. Such an abrupt necking zone is a recurrent feature observed on many other margins. For instance, it is ~150 km on the Galicia continental margin [*Gonzalez et al.*, 1999], ~150 km on the Nova Scotia margin [*Funck et al.*, 2004], ~50 km on the Angolan margin [*Contrucci et al.*, 2004a; *Moulin et al.*, 2005], ~150 km in northern Morocco [*Contrucci et al.*, 2004b], and ~100 km in southern Morocco [*Klingelhoefer et al.*, 2009; *Labails and Olivet*, 2009]. Abrupt crustal thinning, together with a wide basin seaward, can be explained if a vertical collapse of the basin ("sag") occurred. The subsidence may take the form of a seaward tilting with different amplitudes but also the form of a purely vertical movement, without any tilting, as in the case of a "sag" basin. The formation of these wide ("sag") offshore basin (as the SSPS) filled with

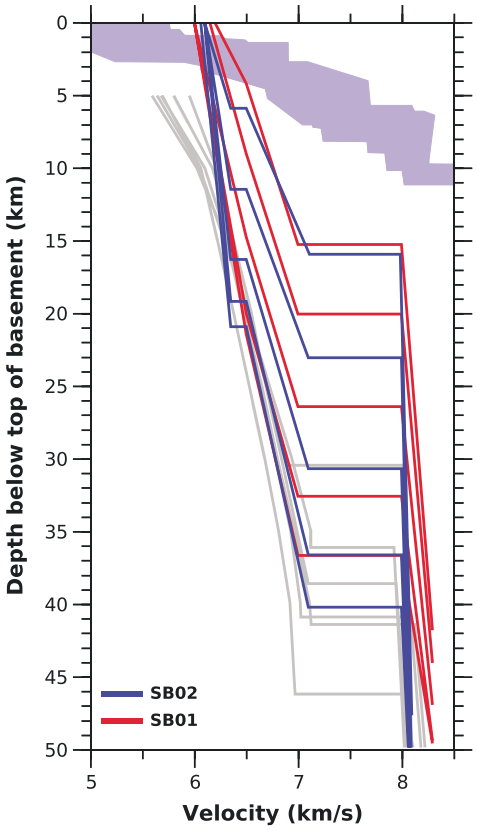

Figure 19. One-dimensional velocity-depth below basement (VZ) profiles at a 25 km interval in Domain N of SB01 (red lines) (−50 to 50 km) and SB02 (blue lines) (−75 to 25 km). The blue shaded area bounds a compilation of velocity profiles for the Atlantic oceanic crust [*White et al*., 1992] while gray profiles correspond to the average velocity profiles of the five tectonic provinces defined by *Christensen and Mooney* [1995] plus their reference profile for continental crust.

quasihorizontal sedimentary layers on top of a continental basement cannot occur if considering a single hinge line and an abrupt thinning of the continental crust. This form of subsidence implies two hinge lines, one located at the beginning (top) and the other at the termination (bottom) of the necking zone [e.g., *Leroux et al*., 2015].

5.4. Structure and Nature of the Crust in Domains A and C

Domains A and C exhibit similar gravity and magnetic patterns with a wide, low gravity anomaly and large positive magnetic anomalies, respectively (Figures 17c and 17d). These two domains also present similar velocity structures with crustal thickness varying between 11 and 17 km and a constant bottom velocity at 7 km/s. The upper layer and velocities are the most changing. The layer is almost absent in places while upper velocities vary between 5.2 and 6.4 km/s. These velocities are globally higher than those found in a previous experiment conducted in the south of the SSPS, where values of 5.09–5.56 km/s and 6.37–6.78 km/s were measured respectively for the upper and lower crustal layers [*Leyden et al*., 1971]. This discrepancy might result from differences in the data acquisition (sonobuoys versus ocean-bottom seismometers) and interpretation methods: older studies used the uniform interval velocities for refracted waves propagating along the layer boundary while modern studies use the more appropriate velocity gradients and rays turning in the different layers [*White et al*., 1992]. Some discrepancies also exist between our models and those interpreted from the MCS data set acquired by ION-GXT [i.e., *Zalán et al*., 2011; *Kumar et al*., 2012]. *Zalán et al*. [2011] state that the Moho rises steeply and mantle is exhumed at the southeastern limit of Domain C and in Domain D. In this area, our velocity models clearly indicate the presence of a Moho discontinuity with a sharp velocity step and an upper mantle at 8.0 km/s, typical for unaltered peridotite. Such observations are incompatible with the presence of exhumed mantle [*Klingelhoefer et al*., 2014]. Also, in geological models of both *Zalán et al*. [2011] and *Kumar et al*. [2012], the position of the Moho is mainly constrained by gravity modeling. Where the SanBa profiles coincide with their models, large differences on the Moho depth can be observed. For example, beneath the boundary between subdomains A and A′ on SB01, the Moho is at 20 km while *Kumar et al*. [2012] place it close to 24 km. In SB01 Domain C, a Moho at 16–17 km has been modeled from seismic data while it is at 23 km depth according to *Zalán et al*. [2011]. Finally, though the Moho depth (22–23 km) in SB02 Domain A is consistent with the one found by *Zalán et al*. [2011], their models suggest progressive thinning of the continental crust in Domain B while a shallow Moho is required by wide-angle data (Figure 21).

The question of the nature of the SSPS has been highly debated [see *Moulin et al*., 2012, for a review]. *Leyden et al*. [1971] concluded on its oceanic nature, while, more recently, *Zalán et al*. [2011] and *Kumar et al*. [2012] interpreted the regions equivalent to Domains A and C as a thinned continental crust. In the reconstruction of *Moulin et al*. [2012], our Domains A and C correspond well to their Domains I and V (except the eastern end of the latter) and partly to their Domains II and IV (Figure 15). They suggest Domains I and V are made of a thinned continental crust. Their Domains II and IV were proposed based

on the termination of presalt sediments and an irregular salt base and presented as either a highly stretched continental crust or exhumed material.

Figures 20a–20c present a compilation of 1-D velocity-depth profiles sampling Domains A and C at every 10 km. None of these curves fit in the bounds of normal oceanic crust [*White et al*., 1992]. They do not either reflect the thickness of typical continental crust [*Christensen and Mooney*, 1995], but the velocity range in both their upper and lower parts is similar to those of typical continental curves as well as those of Domains CC and N. Figures 20d–20f further compare velocity structures between the SSPS and various regions of either continental or oceanic affinity where seismic refraction experiments have imaged similar crustal thicknesses. Domains A and C show a close velocity structure to thinned continental crust imaged at Rockall Trough [*Klingelhöfer et al*., 2005] and along the Sardinian margin [*Afilhado et al*., 2015] (Figure 20d). On the other hand, they differ greatly from thickened oceanic crust found along margins affected by a large amount of volcanism during rifting (e.g., the North Atlantic Volcanic Province [*Parkin and White*, 2008], Figure 20e) and at oceanic plateaus or ridges (e.g., Tuamotu plateau [*Patriat et al*., 2002] or Carnegie Ridge [*Sallarès et al*., 2005], Figure 20f). In these two contexts, both extrusive basalts and a large amount of intruded mafic material explain respectively lower velocities on top of the basement and higher velocities at its base compared to continental crust of similar thickness.

Crustal velocities and structure in Domains A and C and their continuity with the necking zone therefore favor that a vast majority of the SSPS is continental in nature, in good accordance with *Zalán et al*. [2011], *Kumar et al*. [2012], and *Moulin et al*. [2012]. As for Domain N, the highest upper crustal velocity (6.5 km/d) found in Domain A can be explained by a higher density in the crust due to the increased weight of the thickened overlying sediments, by exhumation of middle/lower crust, or a combination of both.

5.5. Structure and Nature of the Crust in Central Domain B

As described above, Domain B has a very heterogeneous crustal structure with an extremely thin crust and the presence of an anomalous velocity layer in its whole northeastern part. It also exhibits very different magnetic and gravimetric patterns compared to Domains A and C. Domain B is comprised in a large area of mostly negative magnetic anomalies (see dashed white line surrounding this area in Figure 17d) and present a v-shaped pattern of positive gravity anomalies (Figure 17c). These observations put into question a single compositional nature for this domain and thus for the entire SSPS. Domain B corresponds partly to Domains II and IV of *Moulin et al*. [2012] and includes their entire Domain III. This domain, which was inferred from changes in salt morphology (from canopy to connected diapirs) and changes in depth of the basement surface and some observed deep reflection patterns, was proposed as an abandoned oceanic ridge.

Figure 22 presents velocity-depth profiles in Domain B. In its southwestern part and along SB02 (Figure 22a), its velocity structure follows the trend discussed above for Domains N, A, and C. Though its thinnest crust falls into the bounds of normal oceanic crust [*White et al*., 1992], the trend argues for the continental nature of the area. This is again in agreement with hypothesis of *Zalán et al*. [2011] except that the crustal thickness found here (7 to 11 km) is far lower than the one (12 to 15 km) supposed by these authors (Figure 21). A 15 km deep Moho is in fact closer to the value found by *Leyden et al*. [1971] who argued for oceanic crust below the SSPS.

In the northeastern part of Domain B (Figures 22b and 22d), velocity-depth profiles are far from those of typical thinned continental crust [*Christensen and Mooney*, 1995] and somehow included into the normal oceanic boundaries defined by *White et al*. [1992]. They differ from profiles in the southwestern part by (1) the presence of a large velocity step (0.5 km/s) at the base of the upper crustal layer, (2) a continuously increasing velocity up to mantle-like values (7.8 km/s), and (3) an absence of velocity step at the Moho (see comparison on Figure 22c). The nature of the crust in Domain B is therefore very different than in the rest of the SSPS. Four hypotheses are discussed below: upper and lower continental crust, oceanic crust, and exhumed mantle.

1. Upper continental crust: A 6.0–6.5 km/s velocity range is too high to support a pure upper continental nature, but it can be explained by the presence of mafic intrusions. Similarly, the high-velocity range (7.0–7.8 km/s) in the anomalous lower layer can be interpreted as lower continental crust with incorporated mafic material. High-velocity lower crust was reported beneath the Angola Margin [*Contrucci et al*., 2004a; *Moulin et al*., 2005], the New Caledonia Basin [*Klingelhoefer et al*., 2007], and the Lake Baikal [*Thybo and Nielsen*, 2009]. In the last two cases, the authors suppose that magmatic material intruded the lower crust, but they still

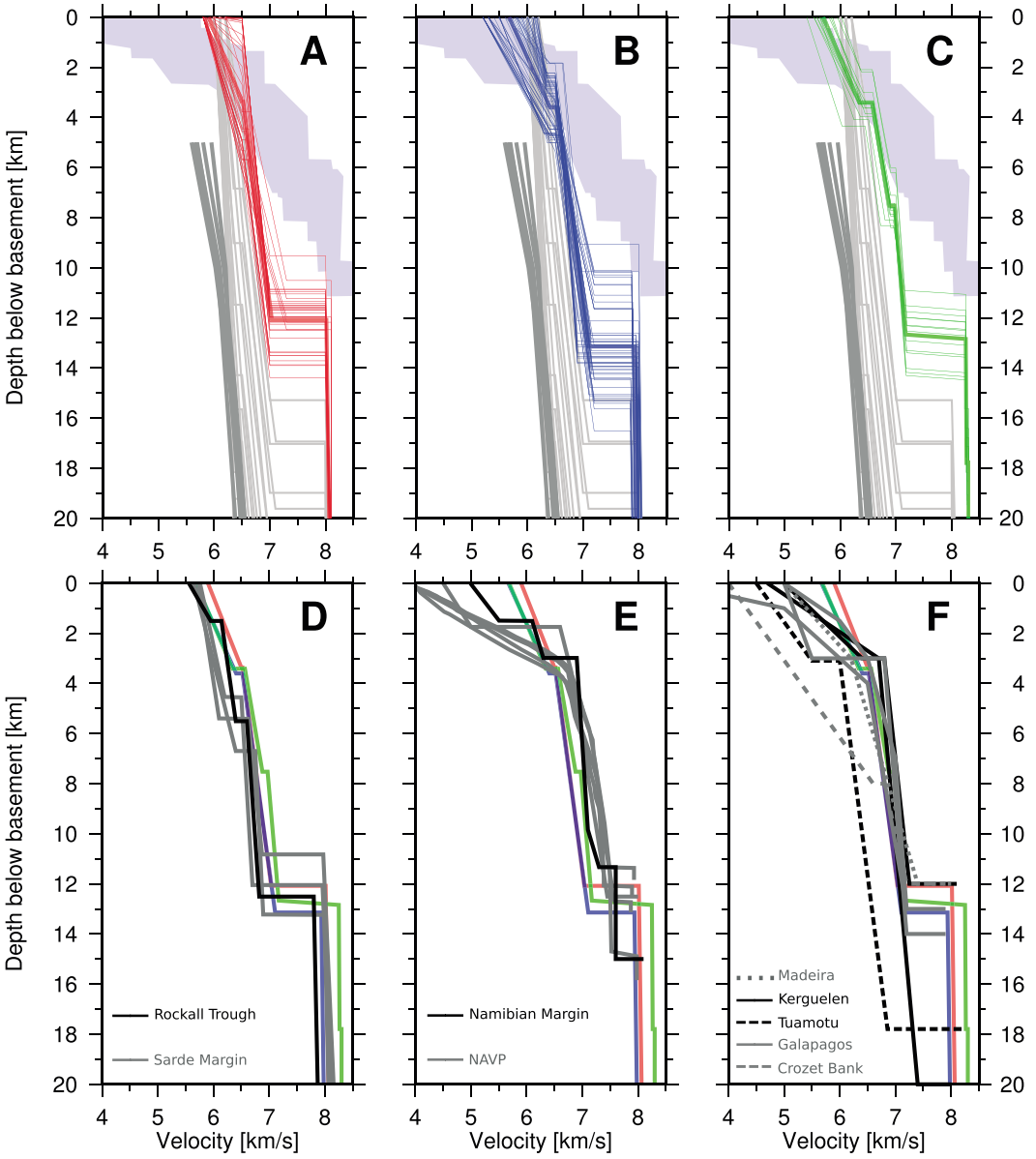

Figure 20. Compilation of 1-D velocity-depth below basement (VZ) profiles spaced every 10 km along Domains A and C in (a) SB01 (60–310 km and 560–600 km) and SB07 (60–100 km), (b) SB02 (30–250 km and 430–620 km) and SB03 (10–130 km from *Klingelhoefer et al.* [2014]), and (c) SB04 (50–180 km). Light gray curves are taken as guidelines from Figure 19 (Domain N). The blue shaded area bounds a compilation of VZ profiles for the Atlantic oceanic crust [*White et al.*, 1992], and gray profiles correspond to the average VZ profiles of the five tectonic provinces defined by *Christensen and Mooney* [1995] plus their reference profile for continental crust. Comparison of mean VZ profiles from Figures 20a (red), 20b (blue), and 20c (green) with VZ profiles from other regions of either (d) continental or (e, f) oceanic crustal affinity where seismic refraction experiments have imaged a similar crustal thickness. In Figure 20d, black: VZ profile at 305 km along Line E imaging Rockall Trough [*Klingelhöfer et al.*, 2005]; gray: VZ profiles at −50 and −60 km along Line GH and 120 km along Line G2H2 imaging the Sardinian Margin [*Afilhado et al.*, 2015]. In Figure 20e, black: VZ profile at 280 km along Transect 2 imaging the Namibian volcanic margin [*Bauer et al.*, 2000]; gray: VZ profiles from the North Atlantic Volcanic Province (NAVP): at 50 and 100 km along the iSIMM line imaging the Faroes margin, at 120 km and 150 km along the iSIMM line imaging the Hatton margin and at 250 km along the SIGMA 3 line imaging the Greenland margins [*Hopper et al.*, 2003; *Parkin and White*, 2008; *White and Smith*, 2009]. In Figure 20f, VZ profiles, black lines for the North Kerguelen and Enderby Basin [*Charvis and Operto*, 1999], dashed black line for the Tuamotu Plateau [*Patriat et al.*, 2002], dashed gray line for the Crozet Bank [*Recq et al.*, 1998], dotted gray line for the Madeira Tore Rise [*Peirce and Barton*, 1991], and gray lines for the Cocos, Carnegie, and Malpelo Ridges [*Sallarès et al.*, 2003, 2005; *Marcaillou et al.*, 2006] in the Galapagos region. Note that the vertical scale represents only the first 20 km of the vertical scale and starts at 4 km/s compared to 5 km/s in Figures 18 and 19.

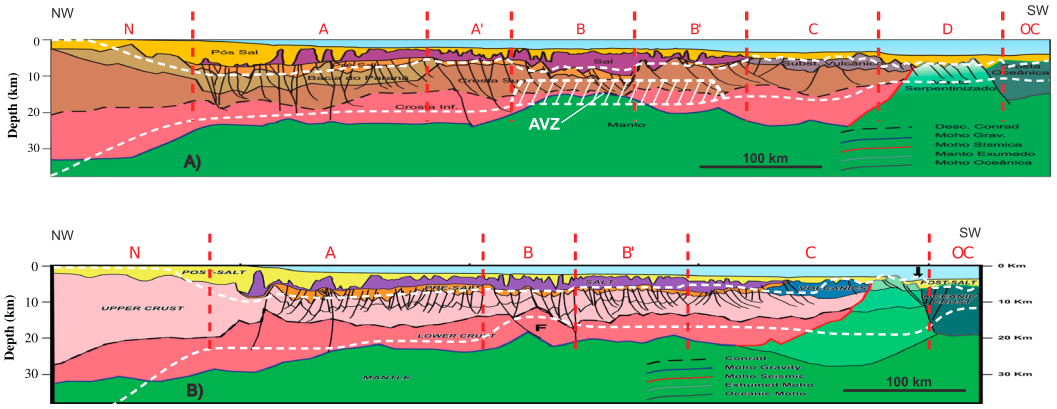

Figure 21. Comparison between geological models of *Zalán et al.* [2011] inferred from GXT seismic lines and gravity modeling and basement structure (dashed white lines) from coincident wide-angle SanBa profiles. (a) GXT line 1575 coincident with SB01; (b) GXT line 1550 coincident with SB02. Names and limits of domains are in red. AVZ: anomalous velocity zone. VE ≈ 3.

observe Moho reflections: the amount of intrusions is not sufficiently important to change the Moho discontinuity into a broad layer of high velocity which would make it transparent. However, neither the strong velocity gradient and a velocity as high as 7.8 km/s is reached in these cases, nor the strong velocity step modeled between the upper and lower crustal layers which is hardly in coherence with a continuous and progressive effect of either increased temperature or mafic intrusions.

2. Exhumed lower continental crust: Exhumed lower continental crust was proposed based on wide-angle seismic data imaging other margins, as the Angola Margin [*Contrucci et al.*, 2004a; *Moulin et al.*, 2005; *Aslanian et al.*, 2009] and Gulf of Lion [*Aslanian et al.*, 2012; *Afilhado et al.*, 2015; *Moulin et al.*, 2015]. Exhumed lower crust were also dredged on the Galician margin [*Whitmarsh and Wallace*, 2001]. In the case where a decoupling exists between the upper and lower crust, such exhumation is reproduced on numerical modeling [*Huismans and Beaumont*, 2011]. Therefore, exhumed lower crust could form part of the transitional

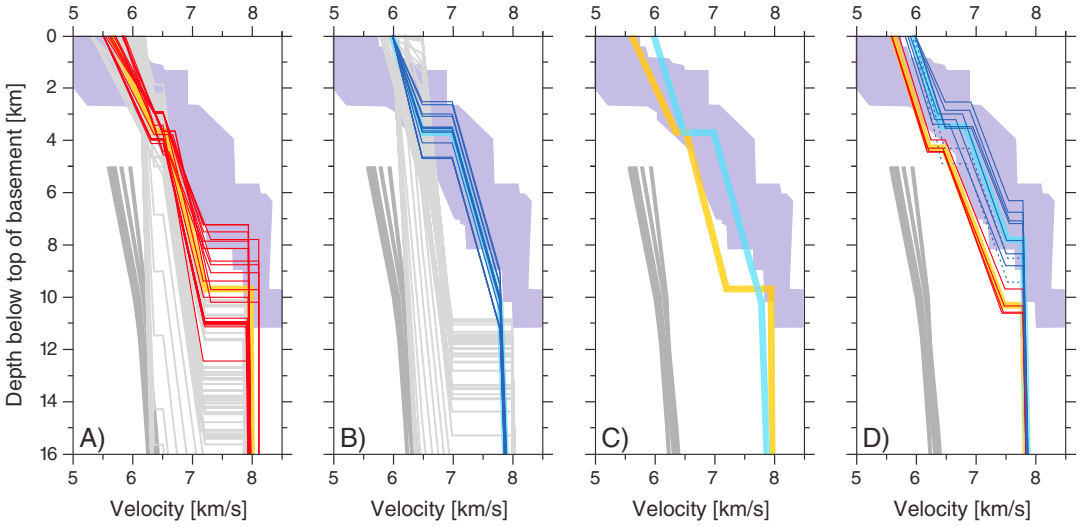

Figure 22. Compilation of 1-D velocity versus depth below basement (VZ) profiles in Domains B and B′. Note that the vertical scale represents only the first 16 km of the vertical scale used in Figure 20. Thin colored lines mark individual VZ profiles at a 10 km interval, and bold lines mean velocity profiles. The blue shaded area bounds a compilation of velocity profiles for the Atlantic oceanic crust [*White et al.*, 1992] while gray profiles correspond to the average velocity profiles of the five tectonic provinces defined by *Christensen and Mooney* [1995] plus their reference profile for continental crust. (a) VZ profiles (in red) in Domains B and B′ of profile SB02 (260–420 km) and Domain B of SB07 (0–60 km)—averaged profile in orange. Light gray lines are SB02 VZ profiles taken as guidelines from Figures 19 (Domain N) and 20b (Domain A and C). (b) VZ profiles (in blue) in Domains B and B′ of profile SB01 (350–480 km)—averaged profile in light blue. Light gray lines are SB01 VZ profiles taken as guidelines from Figures 19 (Domain N) and 20a (Domain A, A′, and C). (c) Comparison of the mean velocity profiles of Figures 22a and 22b. (d) VZ profiles in Domains B′ (0–30 km, in blue) and B (40–120 km, in red) of SB06 with their respective averaged profiles in light blue and orange.

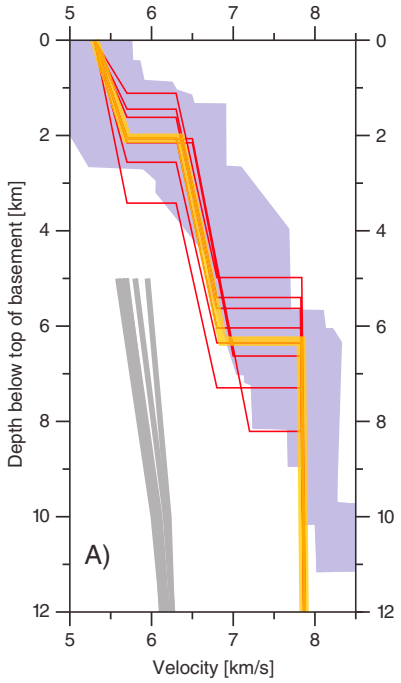

Figure 23. Compilation of 1-D velocity versus depth below basement (VZ) profiles in Domain OC of SB02 (640–710 km in red). Thin lines mark individual VZ profiles at a 10 km interval, and the bold lines the averaged VZ profile in each graph. The blue shaded area bounds a compilation of velocity profiles for the Atlantic oceanic crust [*White et al.*, 1992] while gray profiles correspond to the average velocity profiles of the five tectonic provinces defined by *Christensen and Mooney* [1995] plus their reference profile for continental crust.

crust between purely continental and oceanic crust [*Aslanian et al.*, 2009]. Following *Bott* [1971] and *Aslanian et al.* [2009], *Sibuet and Tucholke* [2012] suggested that the lower crust, which is missing in the palinspastic reconstruction, may flow and feed a first, atypical oceanic crust. In such a case, the high velocities in the lower layer (7.0–7.8 km/s) may represent mantle in an elevated position, altered but not exhumed. A high-velocity layer without a clearly identified Moho was modeled along several margins (e.g., Newfoundland: *Funck et al.* [2003]; Iberia: *Dean et al.* [2000]; Angola: *Contrucci et al.* [2004a]). Many of these studies propose the presence of serpentinized mantle either underlaying continental or oceanic crust or simply exposed beneath a sedimentary cover (exhumed). The assumption behind this interpretation is that the thinning process could allow fracturing and create pathways for seawater to reach the mantle and initiate its serpentinization. Such process would then lower mantle velocities.

3. Oceanic crust: Several studies have hypothesized the presence of either an aborted oceanic propagator [*Mohriak*, 2001; *Mohriak and Szatmari*, 2008; *Mohriak et al.*, 2010] or a failed spreading ridge [*Demercian*, 1996; *Karner*, 2000; *Meisling et al.*, 2001; *Mohriak*, 2001; *Gomes et al.*, 2002, 2009] in the SSPS that would be surrounded by thinned continental crust. Such an episode of seafloor spreading is plausible within the frame of an early stage of opening of the South Atlantic [*Moulin et al.*, 2012]. Two important observations have to be explained to favor the presence of oceanic crust in Domain B. The upper crust layer is indeed thinner (2–4 km thick only), and its velocities are much higher than normal oceanic crust. A thinner than normal oceanic crust can be explained by accretion at a very slow spreading center with insufficient melt supply due to low mantle temperatures [*Bown and White*, 1994]. However, observed velocities look too high (6.0–6.5 km/s) to reflect the presence of oceanic crust layer 2 (3–6.5 km/s). Oceanic layer 3 has a similar velocity range. It has been inferred for a 2 km thick layer of 6.9 km/s—thus much higher than in our models—present in the transition zone of the Newfoundland margin at Flemish Cap [*Funck et al.*, 2003]. This study hypothesized exhumed gabbro at the top of the crust. Such basement exists and has been drilled and dredged over a wide area of the Atlantis Platform at the very slow spreading South West Indian Ridge [*Muller et al.*, 1997]. Finally, the velocity structure of the upper layer in the northeastern Domain B is also very similar to the one found in Domain D. *Klingelhoefer et al.* [2014] show a close fit between the velocity-depth curve of Domain D and those from the extinct spreading center of the Provençal basin [*Gailler et al.*, 2009; *Afilhado et al.*, 2015; *Moulin et al.*, 2015]. If the upper crustal layer in Domain B is indeed oceanic crust, then the anomalous lower layer may solely be altered mantle as discussed in the previous point.
4. Exhumed mantle: Velocities of serpentinized peridotites almost cover the entire range of possible velocities of the crust. It is therefore extremely difficult to fully validate/invalidate this hypothesis without direct evidence. The strong velocity step at the base of the upper layer seems, however, unlikely to be a serpentinization front.

As a summary, the northeastern part of Domain B could consist of an upper layer either oceanic or continental in nature. If oceanic crust is present, it is, however, atypical and without its layer 2 (basalt). On the other hand, if continental crust is present, the upper layer is either made of upper crust with mafic intrusions or exhumed lower crust. In these last two cases, the lower high-velocity layer may be intruded lower continental crust or altered mantle. This last hypothesis is the only one valid in case of overlying oceanic crust.

5.6. Crustal Structure of the Oceanic Crust (Domain OC)

SB02 crosses the Florianópolis Fracture Zone at about 640 km and images about 100 km of oceanic crust (Domain OC). Velocity-depth profiles along this portion of the model (Figure 23) are in good agreement with oceanic crust [*White et al*., 1992], with a mean crustal thickness of 6.3 km. Though this region is less well constrained than the rest of the model, it is worth to note, however, that the Moho was not identified on both MCS and OBS data.

6. Conclusion

The acquisition of deep MCS and wide-angle seismic data during the SanBa experiment allowed the imaging of the crustal structure of the Santos Basin-São Paulo Plateau System (SSPS). Based on the modeling of these data sets, the precise segmentation of the SSPS, in seven distinct domains, is revealed. The ~35–40 km thick continental crust beneath the coast thins to less than 15 km under the shelf along a 100 km wide necking zone. Except in its northeastern central part, thinned continental crust underlies most of the SSPS until normal oceanic crust is reached south of the Florianópolis Fracture Zone. The central part of the SSPS shows a very heterogeneous structure. Toward the NE, the crust changes in less than 100 km from a very thin (7 km) continental structure to a combination of a 2–4 km thick upper layer with velocities between 6.0 and 6.5 km/s overlying an anomalous velocity layer of velocities ranging from 7.0 to 7.8 km/s, characterized by the absence of reflections from the Moho at its base. This structure is interpreted as atypical oceanic crust, exhumed lower continental crust, or intruded upper continental crust, overlying either altered mantle in the first two cases or intruded lower continental crust in the last case. The region appears on the map with a v-shaped segmentation consistent with magnetic and gravimetric fields that suggests an initial episode of rifting within the SSPS that was oblique to the general direction of opening between the South American and African plates.

Contributions

The SanBa Project was led by D. Aslanian and M. Moulin, from Ifremer, and A. Viana, from Petrobras. Modeling of the SanBa profile was done by M. Evain, A. Afilhado, C. Rigotti, A. Loureiro, D. Alves, F. Klingelhoefer, and A. Feld. Processing of the deep-sounding reflection seismic data was done by P. Schnurle. On-land operation was conducted by J. Soares, R. Fuck, M. Vinicius de Lima, L. Matias, and C. Corela. Processing of the high-resolution seismic data was done by M. Benabdellouahed, A. Baltzer, and M. Rabineau.

Acknowledgments

The data set collected during the SanBa experiment is protected under a partnership with Petrobras. Any request has to be addressed to Daniel Aslanian (aslanian@ifremer.fr) and Adriano Viana (avaina@petrobras.com.br). We would like to thank the captain, crew, and MCS technical team of the R/V *L'Atalante*. Many thanks also to the OBS (J. Crozon, P. Pelleau, M. Roudaut, P. Fernagu, D. Le Piver, and R. Apprioual) and land station (M. Paula Ribas and J-L. Duarte) technical teams who made this experiment possible. The GMT [*Wessel and Smith*, 1998] and Seismic Unix software package [*Stockwell*, 1999] were used in the preparation of this paper. We thank editors and reviewers for their comments which substantially improved the manuscript.

References

Afilhado, A., M. Moulin, D. Aslanian, P. Schnurle, F. Klingelhoefer, H. Nouze, M. Rabineau, E. Leroux, and M.-O. Beslier (2015), Deep crustal structure across a young passive margin from wide-angle and reflection seismic data (the SARDINIA experiment)—II Sardinia's margin, *Bull. Soc. Geol. Fr.*, *186*(4–5), 331–351.

Aslanian, D., et al. (2009), Brazilian and African passive margins of the Central Segment of the South Atlantic Ocean: Kinematic constraints, *Tectonophysics*, *468*, 98–112, doi:10.1016/j.tecto.2008.12.016.

Aslanian, D., et al. (2012), Structure and evolution of the Gulf of Lions: The Sardinia seismic experiment and the GOLD (Gulf of Lions Drilling) project, *Leading Edge*, *31*(7), 786–792.

Assumpção, M., D. James, and A. Snoke (2002), Crustal thicknesses in SE Brazilian Shield by receiver function analysis: Implications for isostatic compensation, *J. Geophys. Res.*, *107*(B1), 2156–2202, doi:10.1029/2001JB000422.

Assumpção, M., M. Bianchi, J. Julià, F. L. Dias, G. Sand França, R. Nascimento, S. Drouet, C. G. Pavão, D. F. Albuquerque, and A. E. V. Lopes (2013a), Crustal thickness map of Brazil: Data compilation and main features, *J. South Am. Earth Sci.*, *43*, 74–85, doi:10.1016/j.jsames.2012.12.009.

Assumpção, M., M. Feng, A. Tassara, and J. Julià (2013b), Models of crustal thickness for South America from seismic refraction, receiver functions and surface wave tomography, *Tectonophysics*, *609*, 82–96, doi:10.1016/j.tecto.2012.11.014.

Austin, J. A., Jr., and E. Uchupi (1982), Continental–oceanic crustal transition off Southwest Africa, *AAPG Bull.*, *66*, 1328–1347.

Baltzer, A. et al. (2014), Investigation of different sediment deposits morphologies in the Santos Basin, Brazilian margin, in *RST*, Pau, France.

Bassini, A. (1986), *Levantamentos Sismograficos no Sudeste do Brasil*, Universidade de São Paulo, São Paulo, Brazil.

Bauer, K., S. Neben, B. Schreckenberger, R. Emmermann, K. Hinz, N. Fechner, K. Gohl, S. Albrecht, R. B. Trumbull, and K. Weber (2000), Deep structure of the Namibia continental margin as derived from integrated geophysical studies, *J. Geophys. Res.*, *105*(B11), 25,829–25,853, doi:10.1029/2000JB900227.

Blaich, O. A., J. I. Faleide, and F. Tsikalas (2011), Crustal breakup and continent-ocean transition at South Atlantic conjugate margins, *J. Geophys. Res.*, *116*, B01402, doi:10.1029/2010JB007686.

Bott, M. H. P. (1971), Evolution of young continental margins and formation of shelf basins, *Tectonophysics*, *11*(5), 319–327.

Bown, J. W., and R. S. White (1994), Variation with spreading rate of oceanic crustal thickness and geochemistry, *Earth Planet. Sci. Lett.*, *121*(3–4), 435–449, doi:10.1016/0012-821X(94)90082-5.

Bueno, G. V., D. L. Machado Jr., J. A. Bach de Oliveira, and E. J. J. Marques (2004), A Influencia do Lineamento Capricornio na Evoluco Tectono-Sedimentaria da Bacia de Santos, in *42nd Congresso Brasileiro de Geologia*, Sociedade Brasileira de Geologia, Araxa, Brazil.

Charvis, P., and S. Operto (1999), Structure of the Cretaceous Kerguelen Volcanic Province (southern Indian Ocean) from wide-angle seismic data, *J. Geodyn.*, *28*(1), 51–71, doi:10.1016/S0264-3707(98)00029-5.

Christensen, N. I., and W. D. Mooney (1995), Seismic velocity structure and composition of the continental crust: A global view, *J. Geophys. Res.*, *100*(B7), 9761–9788, doi:10.1029/95JB00259.
Cobbold, P. R., K. E. Meisling, and V. S. Mount (2001), Reactivation of an obliquely rifted margin, Campos and Santos basins, southeastern Brazil, *AAPG Bull.*, *85*(11), 1925–1944.
Contrucci, I., L. Matias, M. Moulin, L. Géli, F. Klingelhoefer, H. Nouzé, D. Aslanian, J.-L. Olivet, J.-P. Réhault, and J.-C. Sibuet (2004a), Deep structure of the West African continental margin (Congo, Zaïre, Angola), between 5°S and 8°S, from reflection/refraction seismics and gravity data, *Geophys. J. Int.*, *158*(2), 529–553, doi:10.1111/j.1365-246X.2004.02303.x.
Contrucci, I., F. Klingelhoefer, J. Perrot, R. Bartolome, M.-A. Gutscher, M. Sahabi, J. Malod, and J.-P. Rehault (2004b), The crustal structure of the NW Moroccan continental margin from wide-angle and reflection seismic data, *Geophys. J. Int.*, *159*, 117–128.
Curie, D. (1984), *Ouverture de l'Atlantique Sud Et Discontinuites Intra-Plaque: Une Nouvelle Analyse*, Universite de Bretagne Occidentale, Brest, France.
Dean, S. M., T. A. Minshull, R. B. Whitmarsh, and K. E. Louden (2000), Deep structure of the ocean-continent transition in the southern Iberia Abyssal Plain from seismic refraction profiles: The IAM-9 transect at 40°20′N, *J. Geophys. Res.*, *105*(B3), 5859–5885, doi:10.1029/1999JB900301.
Demercian, L. S. (1996), *A Halocinese Na Evolução Do Sul da Bacia de Santos do Aptiano ao Cretáceo Superior*, Universidade Federal do Rio Grande do Sul, Porto Alegre, Brazil.
Funck, T., J. R. Hopper, H. C. Larsen, K. E. Louden, B. E. Tucholke, and W. S. Holbrook (2003), Crustal structure of the ocean-continent transition at Flemish Cap: Seismic refraction results, *J. Geophys. Res.*, *108*(B11), 2531, doi:10.1029/2003JB002434.
Funck, T., H. R. Jackson, K. E. Louden, S. A. Dehler, and Y. Wu (2004), Crustal structure of the northern Nova Scotia rifted continental margin (eastern Canada), *J. Geophys. Res.*, *109*, B09102, doi:10.1029/2004JB003008.
Gailler, A., F. Klingelhoefer, J. Olivet, and D. Aslanian (2009), Crustal structure of a young margin pair: New results across the Liguro-Provencal Basin from wide-angle seismic tomography, *Earth Planet. Sci. Lett.*, *286*, 333–345, doi:10.1016/j.epsl.2009.07.001.
Gladczenko, T. P., K. Hinz, O. Eldholm, H. Meyer, S. Neben, and J. Skogseid (1997), South Atlantic volcanic margins, *J. Geol. Soc. Lond.*, *154*, 465–470.
Gomes, P. O., J. Parry, and W. Martins (2002), The outer high of the Santos Basin, Southern São Paulo Plateau, Brazil: Tectonic setting, relation to volcanic events and some comments on hydrocarbon potential, in *AAPG HEDBERG Conference on Hydrocarbon Habitat of Volcanic Rifted Passive Margins*, Stavanger, Norway.
Gomes, P. O., B. Kilsdonk, J. Minken, T. Grow, and R. Barragan (2009), The outer high of the Santos Basin, Southern São Paulo Plateau, Brazil: Pre-salt exploration outbreak, paleogeographic setting, and evolution of the syn-rift structures, *AAPG Search and Discovery Article*, 10193.
Gonçalves De Souza, K. (1991), *La Marge Continentale Bresilienne Sud-Orientale Et Les Domaines Oceaniques Adjacents: Structure Et Evolution*, Universite de Pierre et Marie Curie, Paris, France.
Gonçalves De Souza, K., R. L. Fontana, J. Mascle, J. M. Macedo, W. U. Mohriak, and K. Hinz (1993), The Southern Brazilian margin: An example of a South Atlantic volcanic margin, in *3rd International Congress of the Brazilian Geophysical Society*, pp. 1336–1341, Brazilian Geophys. Soc., Rio de Janeiro, Brazil.
Gonzalez, A., D. Cordoba, and D. Vales (1999), Seismic crustal structure of Galicia continental margin, NW Iberian Peninsula, *Geophys. Res. Lett.*, *26*(8), 1061–1064, doi:10.1029/1999GL900193.
Gradstein, F. M., J. G. Ogg, and A. G. Smith (2004), *A Geologic Time Scale*, Cambridge Univ. Press, Cambridge, U. K.
Heine, C., J. Zoethout, and R. D. Müller (2013), Kinematics of the South Atlantic rift, *Solid Earth*, *4*(2), 215–253, doi:10.5194/se-4-215-2013.
Hekinian, R., T. Juteau, B. Sichler, S. Sichel, G. Udintsev, R. Apprioual, and M. Ligi (2000), Submersible observations of equatorial Atlantic mantle: The St. Paul Fracture Zone region, *Mar. Geol.*, *21*, 529–560.
Hopper, J. R., T. Dahl-Jensen, W. S. Holbrook, H. C. Larsen, D. Lizarralde, J. Korenaga, G. M. Kent, and P. B. Kelemen (2003), Structure of the SE Greenland margin from seismic reflection and refraction data: Implications for nascent spreading center subsidence and asymmetric crustal accretion during North Atlantic opening, *J. Geophys. Res.*, *108*(B5), 2269, doi:10.1029/2002JB001996.
Huismans, R., and C. Beaumont (2011), Depth-dependent extension, two-stage breakup and cratonic underplating at rifted margins, *Nature*, *473*(7345), 74–78, doi:10.1038/nature09988.
Karner, G. D. (2000), Rifts of the Campos and Santos Basins, Southeastern Brazil: Distribution and timing, in *Petroleum Systems of South Atlantic Margins: AAPG Memoir 73*, edited by M. R. Mello and B. J. Katz, pp. 301–315, Am. Assoc. of Petrol. Geol., Tulsa, Okla.
Klingelhöfer, F., R. A. Edwards, R. W. Hobbs, and R. W. England (2005), Crustal structure of the NE Rockall Trough from wide-angle seismic data modeling, *J. Geophys. Res.*, *110*, B11105, doi:10.1029/2005JB003763.
Klingelhoefer, F., Y. Lafoy, J. Collot, E. Cosquer, L. Géli, H. Nouzé, and R. Vially (2007), Crustal structure of the basin and ridge system west of New Caledonia (southwest Pacific) from wide-angle and reflection seismic data, *J. Geophys. Res.*, *112*, B11102, doi:10.1029/2007JB005093.
Klingelhoefer, F., C. Labails, E. Cosquer, S. Rouzo, L. Géli, D. Aslanian, J.-L. Olivet, M. Sahabi, H. Nouzé, and P. Unternehr (2009), Crustal structure of the SW-Moroccan margin from wide-angle and reflection seismic data (the DAKHLA experiment) Part A: Wide-angle seismic models, *Tectonophysics*, *468*, 63–82, doi:10.1016/j.tecto.2008.07.022.
Klingelhoefer, F., et al. (2014), Imaging proto-oceanic crust off the Brazilian continental margin, *Geophys. J. Int.*, *200*(1), 471–488, doi:10.1093/gji/ggu387.
Kumar, N., and L. A. P. Gambôa (1979), Evolution of the São Paulo Plateau (southeastern Brazilian margin) and implications for the early history of the South Atlantic, *Geol. Soc. Am. Bull.*, *90*, 281–293.
Kumar, N., L. A. P. Gamboa, B. C. Schreiber, and J. Mascle (1977), Geologic history and origin of Sao Paulo Plateau (southeastern Brazilian margin), comparison with the Angolan margin, and the early evolution of the northern South Atlantic, in *Initial Reports of the Deep Sea Drilling Project*, vol. 39, edited by P. R. Supko and K. Perch-Nielsen, pp. 927–945, Texas A & M Univ., College Station, Tex.
Kumar, N., A. Danforth, P. Nuttall, J. Helwig, D. E. Bird, and S. Venkatraman (2012), From oceanic crust to exhumed mantle: A 40 year (1970–2010) perspective on the nature of crust under the Santos Basin, SE Brazil, in *Conjugate Divergent Margins*, *Spec. Publ.*, vol. 369, edited by W. U. Mohriak et al., Geol. Soc., London.
Labails, C., and J.-L. Olivet (2009), Crustal structure of the SW Moroccan margin from wide-angle and reflection seismic data (the Dakhla experiment). Part B—The tectonic heritage, *Tectonophysics*, *468*(1–4), 83–97, doi:10.1016/j.tecto.2008.08.028.
Leroux, E., D. Aslanian, M. Rabineau, M. Moulin, D. Granjeon, C. Gorini, and L. Droz (2015), Sedimentary markers in the Provençal Basin (western Mediterranean): A window into deep geodynamic processes, *Terra Nova*, *27*(2), 122–129, doi:10.1111/ter.12139.
Leyden, R., W. J. Ludwig, and M. Ewing (1971), Structure of continental margin off Punta del Este, Uruguay, and Rio de Janeiro, Brazil, *AAPG Bull.*, *55*(12), 2161–2173.
Leyden, R., H. Asmus, S. Zembruscki, and G. Bryan (1976), South Atlantic diapiric structures, *AAPG Bull.*, *60*(2), 196–212.

Leyden, R., J. E. Damuth, L. K. Ongley, J. Kostecki, and W. Van Stevenick (1978), Salt diapirs on Sao Paulo Plateau, southeastern Brazilian continental margin, *AAPG Bull.*, *62*(4), 657–666.
Marcaillou, B., P. Charvis, and J.-Y. Collot (2006), Structure of the Malpelo Ridge (Colombia) from seismic and gravity modelling, *Mar. Geophys. Res.*, *27*(4), 289–300, doi:10.1007/s11001-006-9009-y.
Maus, S., et al. (2009), EMAG2: A 2-arc min resolution Earth magnetic anomaly grid compiled from satellite, airborne, and marine magnetic measurements, *Geochem. Geophys. Geosyst.*, *10*, Q08005, doi:10.1029/2009GC002471.
Meisling, K. E., P. R. Cobbold, and V. S. Mount (2001), Segmentation of an obliquely rifted margin, Campos and Santos Basins, southeastern Brazil, *AAPG Bull.*, *85*(11), 1903–1924.
Mohriak, W. U. (2001), Salt tectonics, volcanic centers, fracture zones and their relationship with the origin and evolution of the South Atlantic Ocean, in *7th International Congress of the Brazilian Geophysical Society*, Brazilian Geophys. Soc., Salvador, Brazil.
Mohriak, W. U. (2004), Recursos energéticos associados à ativação tectônica mesozóico-cenozóica da América do Sul, in *Geologia do Continente Sul-americano: Evolução da Obra de Fernando Flávio Marques de Almeida*, edited by V. Mantesso-Neto et al., pp. 293–318, Beca Produções Culturais Ltda, São Paulo, Brazil.
Mohriak, W. U., and P. Szatmari (2008), Tectónica de Sal, in *Sal, Geologia e Tectónica, Exemplos Nas Bacia Brasileiras*, edited by W. U. Mohriak, P. Szatmari, and S. M. dos Anjos, pp. 90–163, Beca Edices Ltda, São Paulo, Brazil.
Mohriak, W. U., M. Nobrega, M. E. Odegard, B. S. Gomes, and W. G. Dickson (2010), Geological and geophysical interpretation of the Rio Grande Rise, south-eastern Brazilian margin: Extensional tectonics and rifting of continental and oceanic crusts, *Pet. Geosci.*, *16*(3), 231–245, doi:10.1144/1354-079309-910.
Moulin, M., D. Aslanian, J.-L. Olivet, I. Contrucci, L. Matias, L. Géli, F. Klingelhoefer, H. Nouzé, J.-P. Réhault, and P. Unternehr (2005), Geological constraints on the evolution of the Angolan margin based on reflection and refraction seismic data (ZaïAngo project), *Geophys. J. Int.*, *162*, 793–810.
Moulin, M., D. Aslanian, and P. Unternehr (2010), A new starting point for the South and Equatorial Atlantic Ocean, *Earth Sci. Rev.*, *98*, 1–37, doi:10.1016/j.earscirev.2009.08.001.
Moulin, M., D. Aslanian, M. Rabineau, M. Patriat, and L. Matias (2012), Kinematic keys of the Santos-Namibe basins, in *Conjugate Divergent Margins*, *Spec. Publ.*, vol. 369, edited by W. U. Mohriak et al., Geol. Soc., London.
Moulin, M., F. Klingelhoefer, A. Afilhado, D. Aslanian, P. Schnurle, H. Nouze, M. Rabineau, M.-O. Beslier, and A. Feld (2015), Deep crustal structure across a young passive margin from wide-angle and reflection seismic data (The SARDINIA Experiment)—I Gulf of Lion's margin, *Bull. Soc. Geol. Fr.*, *186*(4–5), 309–330.
Muller, M. R., C. J. Robinson, T. A. Minshull, R. S. White, and M. J. Bickle (1997), Thin crust beneath ocean drilling program borehole 735B at the Southwest Indian Ridge?, *Earth Planet. Sci. Lett.*, *148*(1–2), 93–107, doi:10.1016/S0012-821X(97)00030-7.
Nürnberg, D., and R. D. Müller (1991), The tectonic evolution of the South Atlantic from Late Jurassic to present, *Tectonophysics*, *191*, 27–53, doi:10.1016/0040-1951(91)90231-G.
Olivet, J.-L., J. Bonnin, P. Beuzart, and J.-M. Auzende (1984), *Cinématique de l'Atlantique Nord et Central, Rapports Scientifiques et Techniques*, Centre National pour l'Exploitation des Oceans, Brest, France.
Parkin, C. J., and R. S. White (2008), Influence of the Iceland mantle plume on oceanic crust generation in the North Atlantic, *Geophys. J. Int.*, *173*(1), 168–188, doi:10.1111/j.1365-246X.2007.03689.x.
Patriat, M., F. Klingelhoefer, D. Aslanian, I. Contrucci, M.-A. Gutscher, J. Talandier, F. Avedik, J. Francheteau, and W. Weigel (2002), Deep crustal structure of the Tuamotu plateau and Tahiti (French Polynesia) based on seismic refraction data, *Geophys. J. Int.*, *29*(14), 1-1–1-4, doi:10.1029/2001GL013913.
Peirce, C., and P. J. Barton (1991), Crustal structure of the Madeira Tore Rise, eastern North Atlantic results of a DOBS wide angle and normal incidence seismic experiment in the Josephine Seamount region, *Geophys. J. Int.*, *106*, 357–378.
Perch-Nielsen, K., P. R. Supko, A. Boersma, R. L. Carlson, M. G. Dinkelman, R. V. Fodor, N. Kumar, F. Mccoy, J. Thiede, and H. B. Zimmerman (1977), Site 356: São Paulo Plateau, in *Initial Reports of the Deep Sea Drilling Project*, vol. 39, pp. 141–230, U.S. Gov. Off., Wash.
Péron-Pinvidic, G., and G. Manatschal (2008), The final rifting evolution at deep magma-poor passive margins from Iberia-Newfoundland: A new point of view, *Int. J. Earth Sci.*, *98*(7), 1581–1597, doi:10.1007/s00531-008-0337-9.
Rabinowitz, P. D., and J. Labrecque (1979), The Mesozoic South Atlantic Ocean and evolution of its continental margins, *J. Geophys. Res.*, *84*, 5973–6002.
Recq, M., J. Goslin, P. Charvis, and S. Operto (1998), Small-scale crustal variability within an intraplate structure: The Crozet Bank (southern Indian Ocean), *Geophys. J. Int.*, *134*, 145–156, doi:10.1046/j.1365-246X.1998.00530.x.
Sallarès, V., P. Charvis, E. R. Flueh, and J. Bialas (2003), Seismic structure of Cocos and Malpelo Volcanic Ridges and implications for hot spot-ridge interaction, *J. Geophys. Res.*, *108*(B12), 2564, doi:10.1029/2003JB002431.
Sallarès, V., P. Charvis, E. R. Flueh, and J. Bialas (2005), Seismic structure of the Carnegie ridge and the nature of the Galápagos hotspot, *Geophys. J. Int.*, *161*(3), 763–788, doi:10.1111/j.1365-246X.2005.02592.x.
Sandwell, D. T., and W. H. F. Smith (2009), Global marine gravity from retracked Geosat and ERS-1 altimetry: Ridge segmentation versus spreading rate, *J. Geophys. Res.*, *114*, B01411, doi:10.1029/2008JB006008.
Seyler, M., and E. Bonatti (1997), Regional-scale melt-rock interaction in lherzolitic mantle in the Romanche Fracture Zone (Atlantic Ocean), *Earth Planet. Sci. Lett.*, *146*(1–2), 273–287, doi:10.1016/S0012-821X(96)00220-8.
Sibuet, J.-C., and B. E. Tucholke (2012), The geodynamic province of transitional lithosphere adjacent to magma-poor continental margins, in *Conjugate Divergent Margins*, *Spec. Publ.*, vol. 369, edited by W. U. Mohriak et al., Geol. Soc., London.
Smith, W. H. F., and D. T. Sandwell (1997), Global Sea Floor Topography from Satellite Altimetry and Ship Depth Soundings, *Science*, *277*, 1956–1962.
Stockwell, J. W., Jr. (1999), The CWP/SU: Seismic Un x package, *Comput. Geosci.*, *25*(4), 415–419, doi:10.1016/S0098-3004(98)00145-9.
Thybo, H., and C. A. Nielsen (2009), Magma-compensated crustal thinning in continental rift zones, *Nature*, *457*(7231), 873–876, doi:10.1038/nature07688.
Torsvik, T. H., S. Rousse, C. Labails, and M. A. Smethurst (2009), A new scheme for the opening of the South Atlantic Ocean and the dissection of an Aptian salt basin, *Geophys. J. Int.*, *177*, 1315–1333, doi:10.1111/j.1365-246X.2009.04137.x.
Unternehr, P., J.-L. Olivet, J. Goslin, and P. Beuzart (1988), South Atlantic fits and intrastate boundaries in Africa and South America, *Tectonophysics*, *155*, 169–179.
Wessel, P., and W. H. F. Smith (1998), New, improved version of the Generic Mapping Tools released, *Eos Trans. AGU*, *79*(47), 579.
White, R. S., and L. K. Smith (2009), Crustal structure of the Hatton and the conjugate east Greenland rifted volcanic continental margins, NE Atlantic, *J. Geophys. Res.*, *114*, B02305, doi:10.1029/2008JB005856.
White, R. S., D. McKenzie, and R. K. O'Nions (1992), Oceanic crustal thickness from seismic measurements and rare earth elements inversions, *J. Geophys. Res.*, *97*(B13), 19,683–19,715, doi:10.1029/92JB01749.

Whitmarsh, R. B., and P. J. Wallace (2001), The rift-to-drift development of the west Iberia nonvolcanic continental margin: A summary and review of the contribution of Ocean Drilling Program Leg 173, in *Proceedings of the Ocean Drilling Program, Scientific Results*, vol. 173, edited by M.-O. Beslier et al., pp. 1–36, Ocean Drilling Program, College Station, Tex.

Whitmarsh, R. B., R. S. White, S. J. Horsefield, J.-C. Sibuet, M. Recq, and V. Louvel (1996), The ocean-continent boundary off the western continental margin of Iberia: Crustal structure west of Galicia Bank, *J. Geophys. Res.*, *101*(B12), 28,291–28,314, doi:10.1029/96JB02579.

Zalán, P. V., M. d. C. G. Severino, C. A. Rigoti, L. P. Magnavita, J. A. B. De Oliveira, and A. R. Vianna (2011), An entirely new 3D-view of the crustal and mantle structure of a South Atlantic Passive Margin—Santos, Campos and Espírito Santo Basins, Brazil, in *AAPG Annual Convention and Exhibition*, Houston, Texas.

Zelt, C. A. (1999), Modelling strategies and model assessment for wide angle seismic traveltime data, *Geophys. J. Int.*, *139*, 183–204.

Zelt, C. A., and R. B. Smith (1992), Seismic traveltime inversion for 2-D crustal velocity structure, *Geophys. J. Int.*, *108*, 16–34.

Journal of Geophysical Research: Solid Earth

Supporting Information for

Deep structure of the Santos Basin-São Paulo Plateau System, SE Brazil

M. Evain[1], A. Afilhado[1,2,3], C. Rigoti[4], A. Loureiro[2], D. Alves[2], F. Klingelhoefer[1], P. Schnurle[1], A. Feld[1], R. Fuck[5], J. Soares[5], M. Vinicius de Lima[6], C. Corela[2], L. Matias[2], M. Benabdellouahed[1,7], A. Baltzer[1,8], M. Rabineau[7], A. Viana[4], M. Moulin[1], D. Aslanian[1]

[1]Ifremer, REM-GM-Laboratoire de Géodynamique et de Géophysique (LGG), Technopôle Brest-Iroise, CS 10070, 29280 Plouzane, France, [2]Instituto Dom Luis (IDL), Faculdade de Ciências da Universidade de Lisboa, 1749-016 Lisboa, Portugal, [3]Instituto Superior de Engenharia de Lisboa (ISEL), Rue Conselheiro Emidio Navarro, 1959-007 Lisboa, Portugal, [4]PETROBRAS/CENPES-PROFEX, Rio de Janeiro, Brazil, [5]Lablithos, Instituto de Geociências (IG), Universidade de Brasilia, Campus Darcy Ribeiro, 70910-900 Brasilia, Brazil, [6]Universidade Federal do Pampa, Campus Caçapava do Sul, Caçapava do Sul, Brazil, [7]Institut universitaire européen de la mer (IUEM), Domaines Océaniques, CNRS, 29280 Plouzané, France, [8]LETG-Nantes Géolittomer, Université de Nantes, Campus Tertre, BP 81227 - 44312 Nantes, Cedex 3, France

Contents of this file

Introduction

The Multi-Channel Seismic (MCS) and Ocean Bottom Seismometer (OBS) datasets used in this study was recorded during the Sanba Experiment. Wide-angle data were modeled using the ray tracing and two-dimensional iterative damped least-squares travel-time inversion RAYINVR software [Zelt & Smith, 1992; Zelt, 1999]. Here we provide figures and tables that were used to model and assess final velocity models.

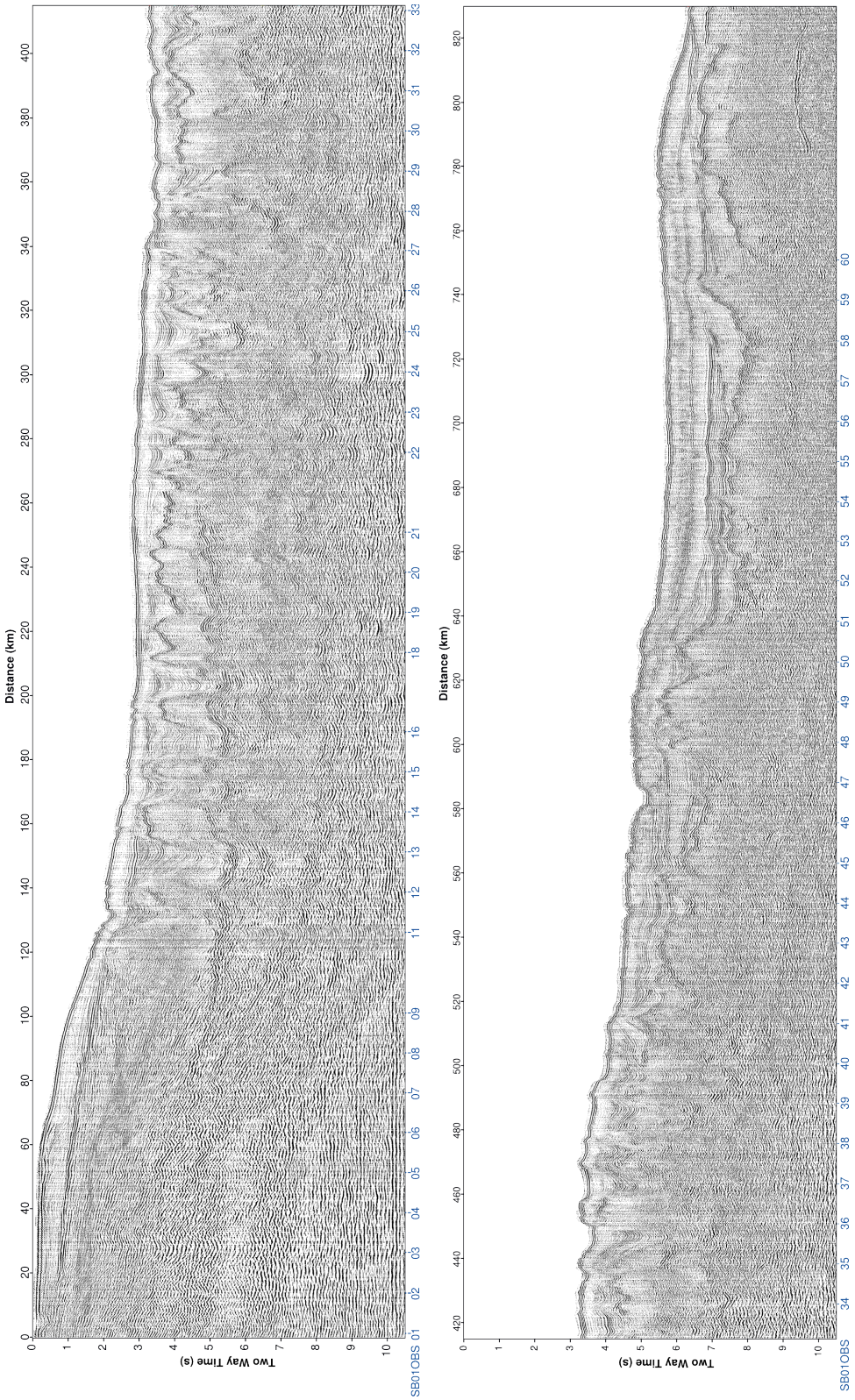

Figure S1a. SB01 MCS profile filtered with FX-deconvolution and plotted in true amplitude.

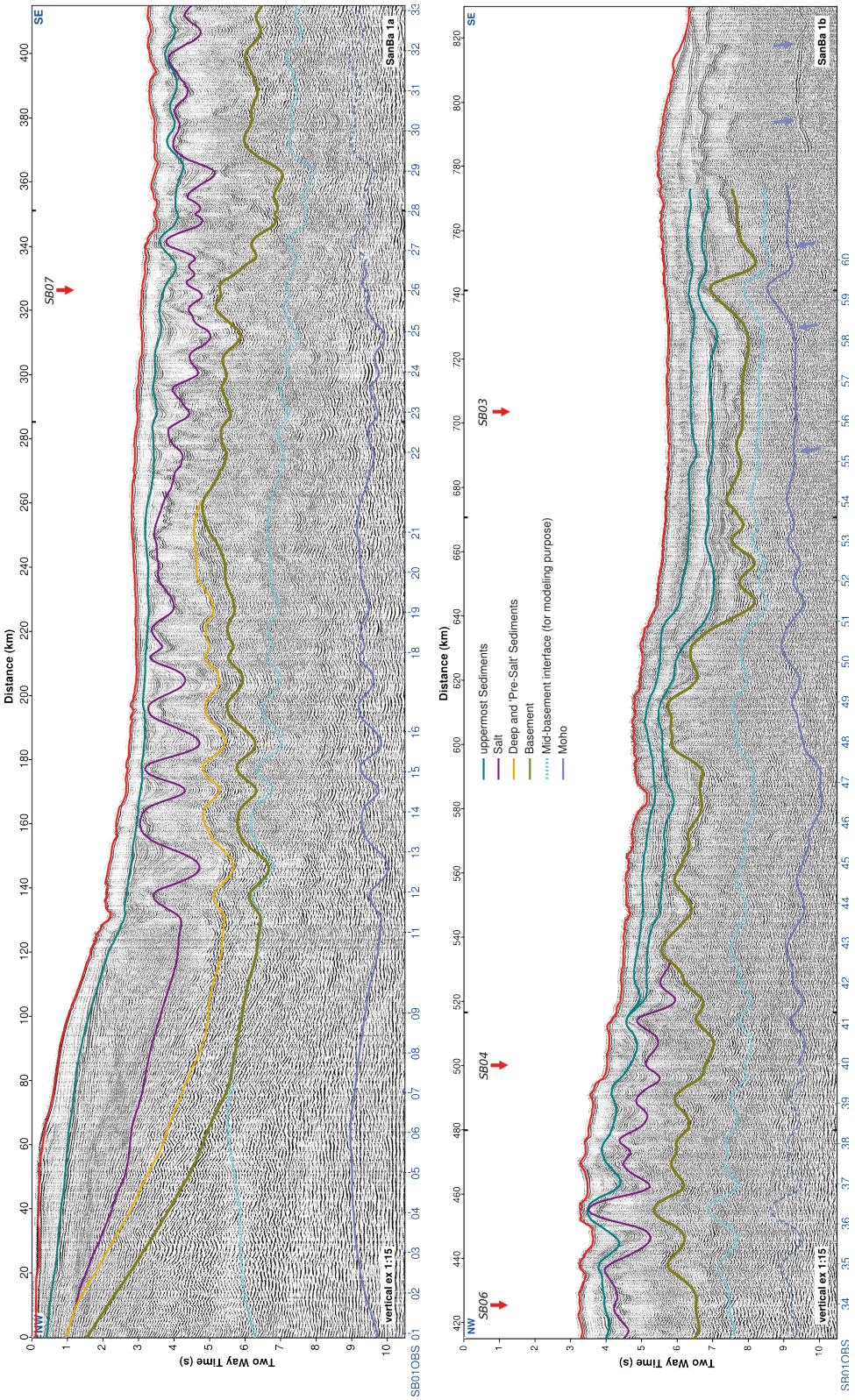

Figure S1b. SB01 MCS profile (same as above) overlain by color coded lines (see inset) that correspond to the interfaces of coincident wide-angle velocity model. Crossings with other SB profiles are indicated by red arrows.

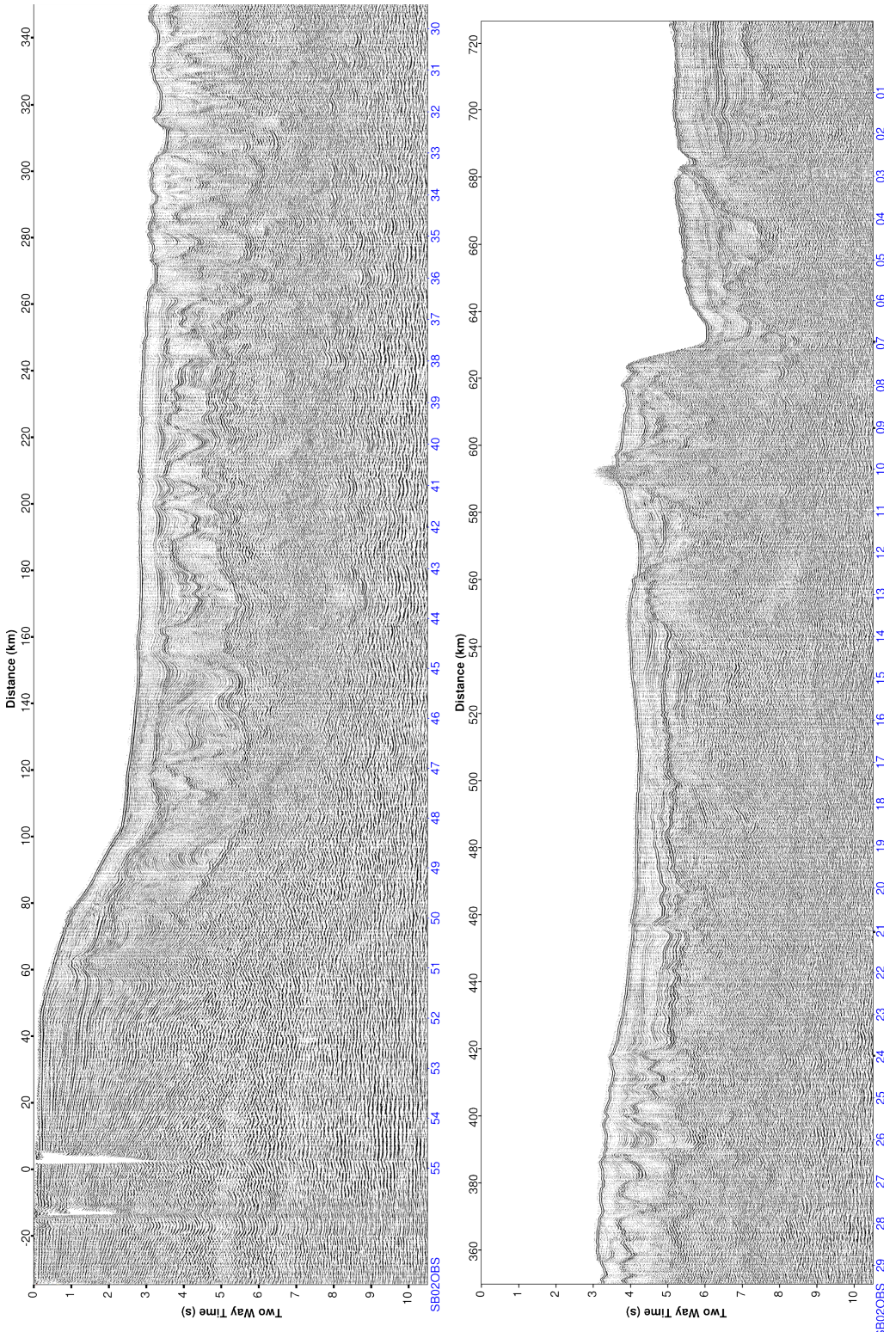

Figure S2a. SB02 MCS profile filtered with FX-deconvolution and plotted in true amplitude.

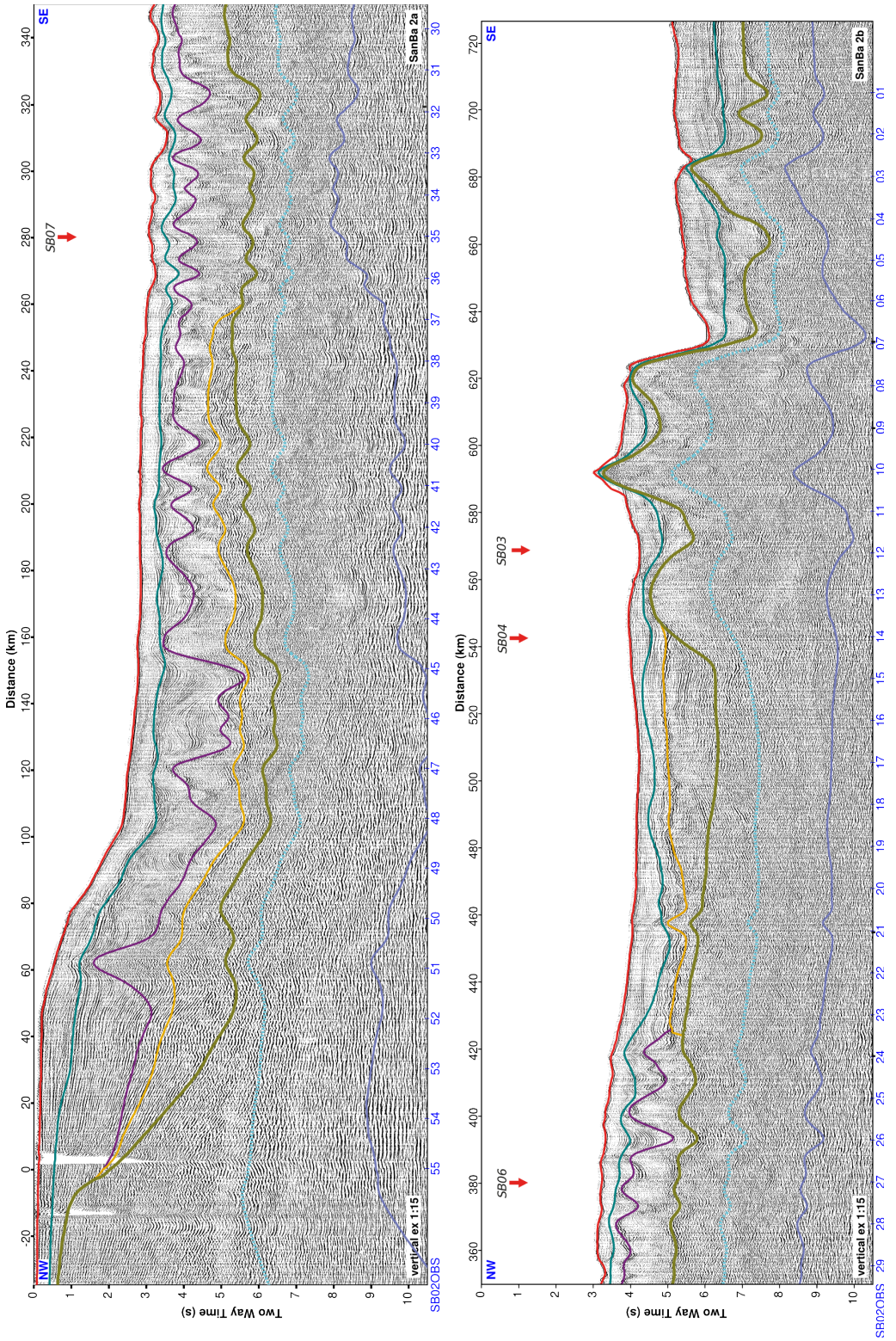

Figure S2b. SB02 MCS profile (same as above) overlain by color coded lines (see inset in Figure S1b) that correspond to the interfaces of coincident wide-angle velocity model. Crossings with other SB profiles are indicated by red arrows.

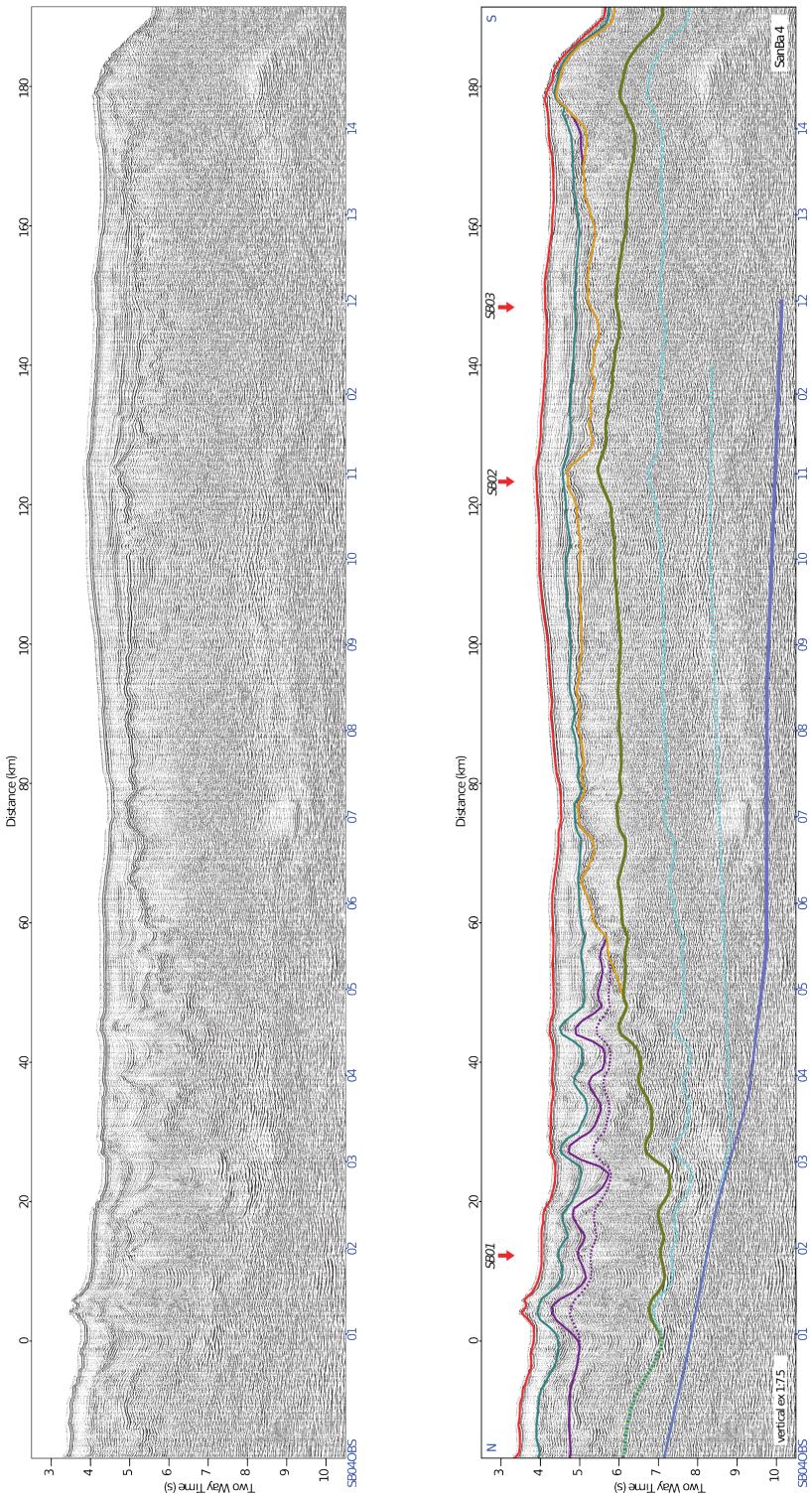

Figure S3 (left) SB04 MCS profile filtered with FX-deconvolution and plotted in true amplitude. (Right) Same profile overlain by color coded lines (see inset in Figure S1b) that correspond to the interfaces of coincident wide-angle velocity model. Crossings with other SB profiles are indicated by red arrows.

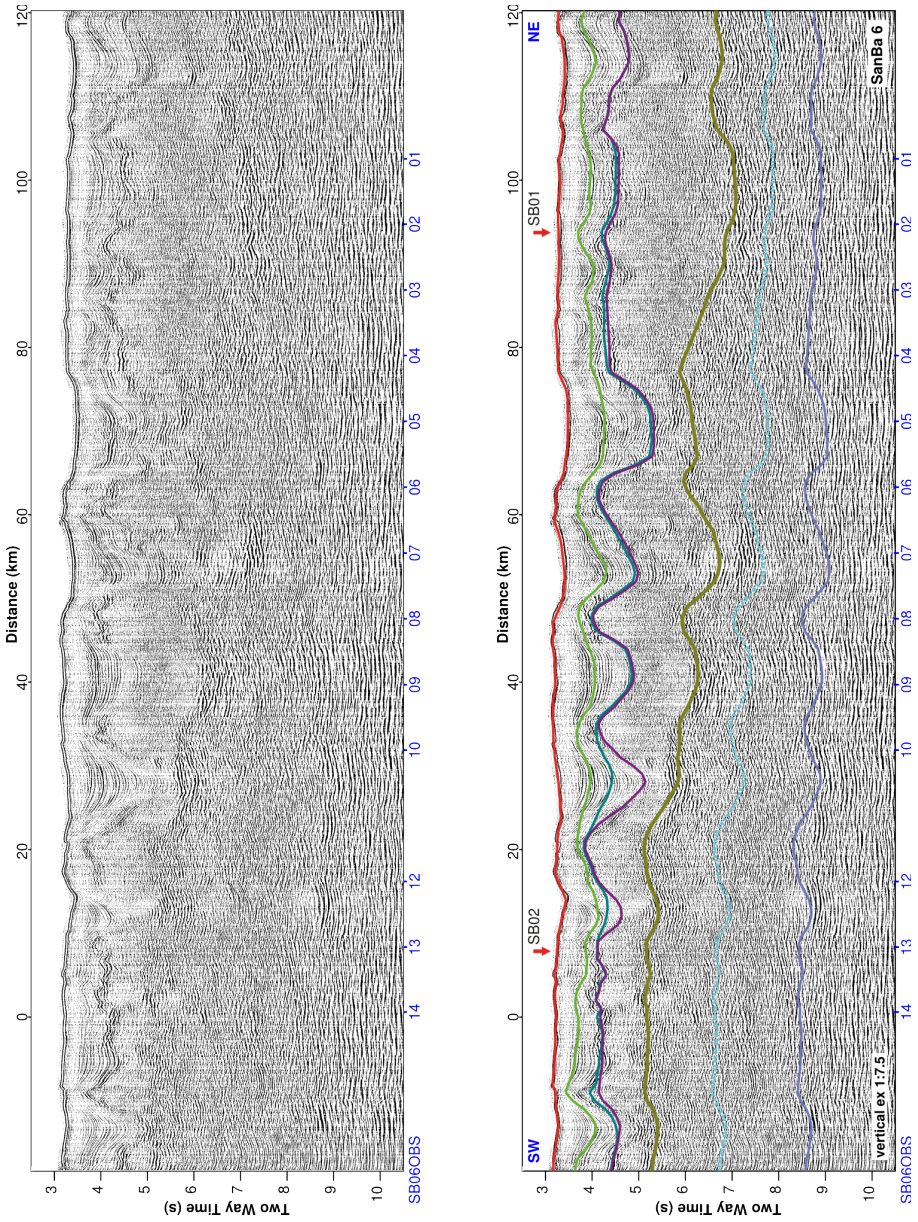

Figure S4. (left) SB06 MCS profile filtered with FX-deconvolution and plotted in true amplitude. (Right) Same profile overlain by color coded lines (see inset in Figure S1b) that correspond to the interfaces of coincident wide-angle velocity model. Crossings with other SB profiles are indicated by red arrows.

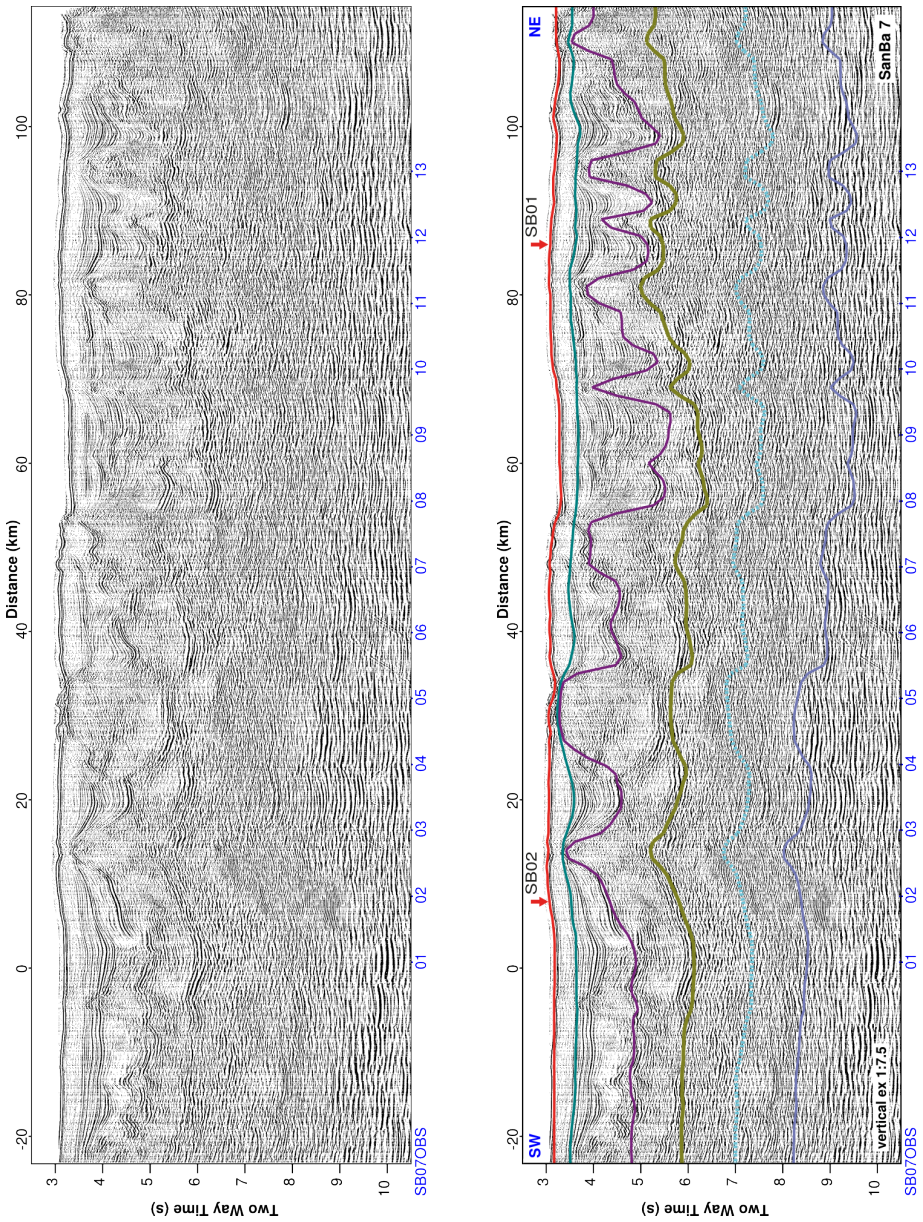

Figure S5. (left) SB07 MCS profile filtered with FX-deconvolution and plotted in true amplitude. (Right) Same profile overlain by color coded lines (see inset in Figure S1b) that correspond to the interfaces of coincident wide-angle velocity model. Crossings with other SB profiles are indicated by red arrows.

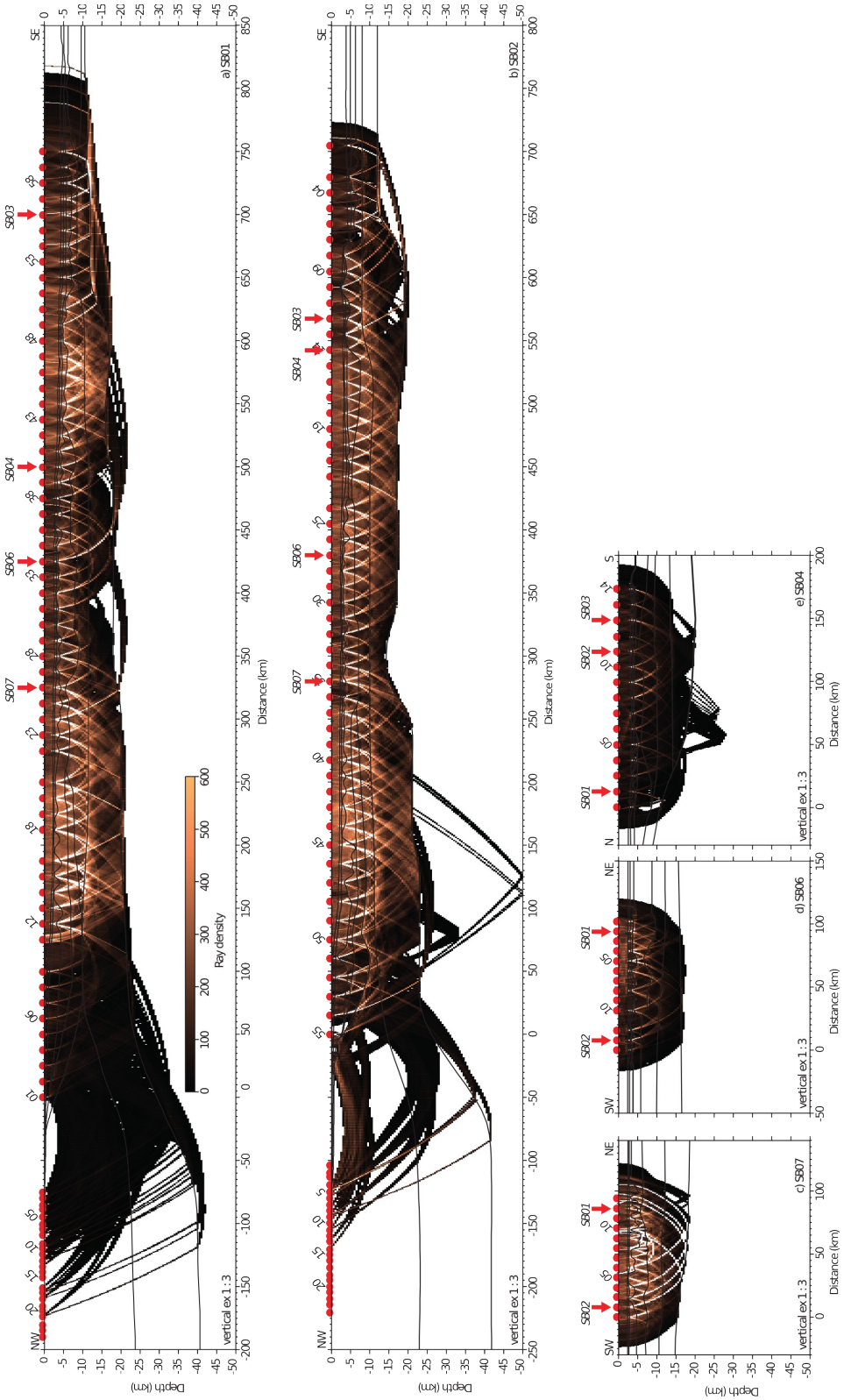

Figure S6. Ray density along a) SB01, b) SB02, c) SB04, d) SB06, e) SB07.

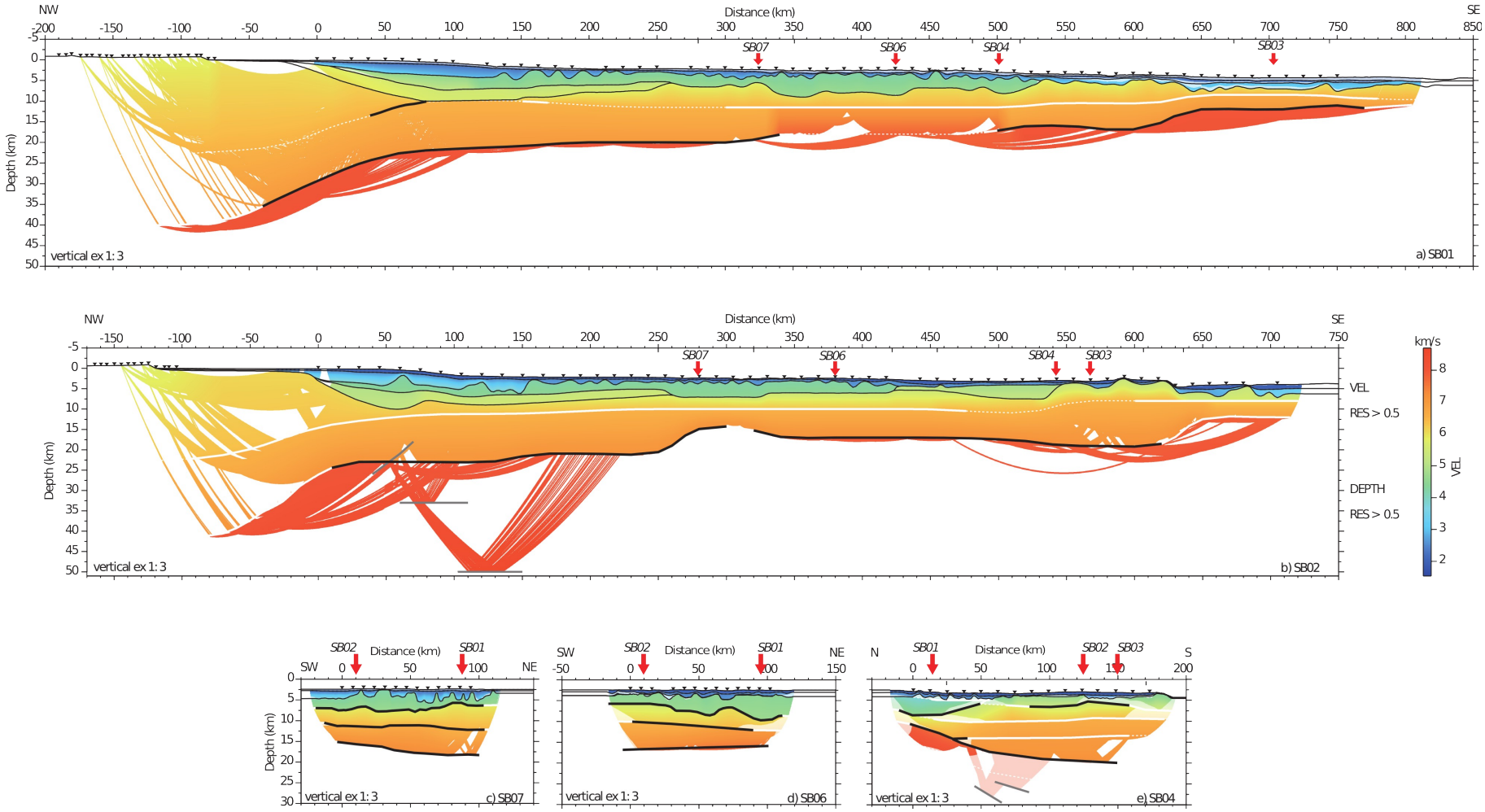
NW
SE
Distance (km)
Depth (km)
SB07
SB06
SB04
SB03
vertical ex 1: 3
a) SB01
b) SB02
VEL
RES > 0.5
DEPTH
RES > 0.5
km/s
VEL
SW
NE
SB02
SB01
c) SB07
d) SB06
N
S
e) SB04

Figure S7. Results of resolution tests for a priori velocity uncertainty of 0.1 km/s and depth uncertainty of 1 km in a) SB01, b) SB02, c) SB04, d) SB06, e) SB07. White regions are not imaged by seismic rays, light colors indicate regions that have resolution values for velocity less than 0.5 and are considered as unresolved. Similarly, some interfaces appear either as dashed or continuous white lines whether their depth is unresolved (value < 0.5) or resolved (value >= 0.5). Among the latter, those superposed by a thick black line indicate where wide-angle reflections hit the interface. This mathematical test has not been applied on the upper interfaces displayed as thin black lines as they were already constrained by MCS data.

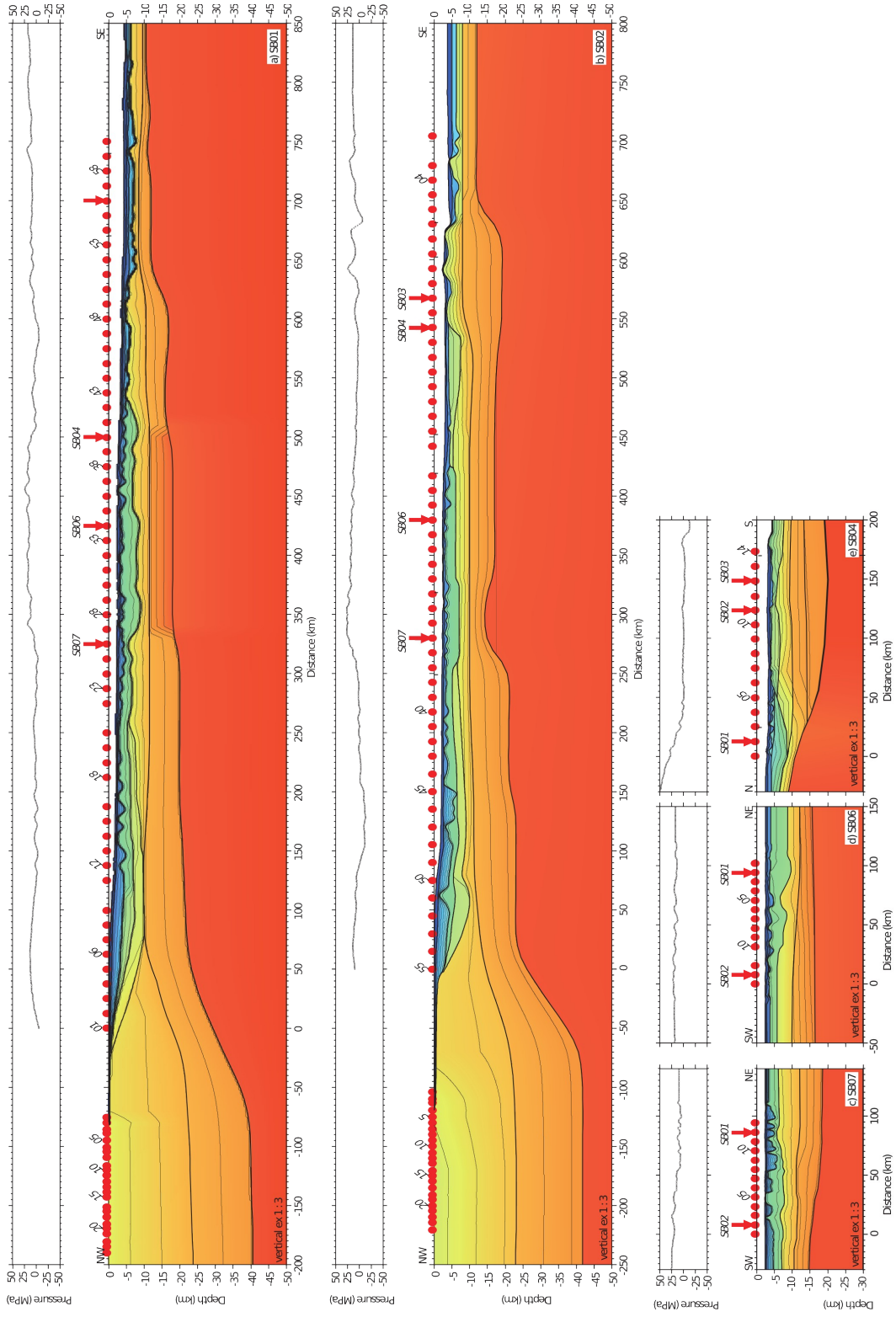

Figure S8. Lithospheric pressure computed along a) SB01, b) SB02, c) SB04, d) SB06, e) SB07.

Phase name SB01	Number of picks	RMS error (ms)	χ2
Water	3756	33	0.2
Refractions in Sediments	1393	135	2.1
Reflections from Sediments	3360	50	0.28
Reflections on top of the Salt	3243	138	1.92
Refractions in Salt	5473	146	2.436
Reflections on top of the Pre-Salt	5340	125	1.506
Refractions in Pre-Salt	1829	169	2.713
Reflections on the basement	1764	142	1.618
Refractions in upper crustal layer	13475	139	1.87
Reflections on top of lower crustal layer	184	209	4.4
Refractions in lower crustal layer	13948	163	1.81
PmP	12732	168	2.26
Pn	7030	309	5.12
Number total of picks	73527		
RMS for all travel-times		167	
Normalized χ2 for SB01			2.12

Table S1. Number of picks, rms error and χ^2 value for each phase modeled in wide-angle model SB01.

Phase name SB02	Number of picks	RMS error (ms)	χ2
Water	3301	72	0.79
Refractions in Sediments	1673	164	3.73
Reflections from Sediments	2202	66	0.65
Reflections on top of the Salt	1775	92	1.16
Refractions in Salt	4202	153	2.832
Reflections on top of the Pre-Salt	4456	119	1.605
Refractions in Pre-Salt & Basin	3339	141	2.091
Reflections on the Pre-salt and Basin	1163	140	1.913
Refractions in upper crustal layer	10821	134	1.94
Refractions in lower crustal layer	15429	136	1.64
PmP	11363	153	1.79
Pn	1800	287	7.28
Reflections from the mantle	206	280	8.51
Number of picks	61730		
RMS travel-time residual		143	
Normalized χ2 for SB02			1.98

Table S2. Number of picks, rms error and χ^2 value for each phase modeled in wide-angle model SB02.

Phase name SB04	Number of picks	RMS error (ms)	χ2
Water	6503	109	1.19
Reflections and Refractions in Sediments 1	248	102	1.88
Reflections and Refractions in Sediments 2	792	53	0.51
Reflections and Refractions in Salt	676	98	1.72
Refracted in the Basin	1075	84	1.244
Reflected on top of the Basement	298	137	3.35
Pg	7720	91	1.48
PmP	1560	98	1.71
Pn	605	144	3.7
Reflected from the mantle	396	69	0.85
Number of picks	13122		
RMS travel-time residual		96	
Normalized χ2 for SB04			1.64

Table S3. Number of picks, rms error and χ^2 value for each phase modeled in wide-angle model SB04.

Phase name SB06	Number of picks	RMS error (ms)	χ2
Water	2598	24	0.227
Reflection Sediments 1	345	58	1.35
Refraction Sediments 2	283	80	2.54
Reflection Sediments 2	376	96	3.67
Refraction Salt	1314	115	5.3
Reflections on top of Basement	817	92	3.42
Upper crustal layer	1411	148	8.76
Reflections on top of lower crustal layer	203	109	4.75
Lower crustal layer	1801	172	11.79
PmP	328	107	4.62
Pn	153	183	13.52
Number of data points	9629		
RMS travel-time residual		115	
Normalized χ2 for SB06			5.3

Table S4. Number of picks, rms error and χ^2 value for each phase modeled in wide-angle model SB06.

Phase name SB07	Number of picks	RMS error (ms)	χ2
Water	798	24	0.06
Reflections in Sediments	416	53	0.28
Refractions in Sediments	1193	214	4.58
Reflections on top of Salt	2425	76	0.59
Refractions in Salt	272	256	6.59
Reflections on top of Basement	2675	115	1.32
Refractions in Upper crustal layer	2948	111	1.24
Reflections on top of lower crustal layer	1304	73	0.53
Refractions in Lower crustal layer	133	0.15	2.16
PmP	3613	129	1.66
Number of picks	15777		
RMS travel-time residual		121	
Normalized χ2 for SB07			1.46

Table S5. Number of picks, rms error and χ^2 value for each phase modeled in wide-angle model SB07.

References:

Zelt, C. A. (1999), Modelling strategies and model assessment for wide angle seismic traveltime data, *Geophysical Journal International*, *139*, 183–204.

Zelt, C. A., and R. B. Smith (1992), Seismic traveltime inversion for 2-D crustal velocity structure, *Geophysical Journal International*, *108*, 16–34.